The Pennsylvania State University

The Graduate School

Department of Chemistry

THE ROLE OF METAL ELECTRODE AND NANOPARTICLE SURFACE FUNCTIONALIZATION IN A HYBRID BIOLOGICAL/ORGANIC DEVICE FOR HYDROGEN PRODUCTION

A Thesis in

Chemistry

by

Rebecca A. Grimme

Submitted in Partial Fulfillment
of the Requirements
for the Degree of

Master of Science

December 2009

The thesis of Rebecca A. Grimme was reviewed and approved* by the following:

John H. Golbeck
Professor of Biochemistry and Biophysics
Thesis Advisor

William G. Noid
Assistant Professor of Chemistry

Raymond E. Schaak
Associate Professor of Chemistry

Barbara J. Garison
Head of the Chemistry Department
Shapiro Professor of Chemistry

*Signatures are on file in the Graduate School

ABSTRACT

The generation of H_2 by solar energy conversion is a promising way to supply the world's energy needs as a means to supplant fossil fuels. All photocatalytic systems contain 3 components: a photochemical module that harnesses the sun's energy, a catalytic module that generates H_2, and a means of linking the two modules together. To this end a hybrid biological system has been designed that incorporates a dithiol molecular wire to connect the terminal [4Fe-4S] cluster of Photosystem I (the photochemical module) with either a Pt or Au nanoparticle (the catalytic module). The sulfhydryl group at one end of the molecular wire allows for the functionalization the nanoparticles via a metal-sulfide (either Au-S or Pt-S) bond and the other sulfhydryl group can chemically rescue the [4Fe-4S] cluster, of Photosystem I, thereby generating a strong coordination bond. The use of sacrificial electron donors enables this bioconjugate system to evolve H_2 when continuously illuminated.

In an effort to maximize H_2 production, the pH and ionic concentration of the solution, the mobility of the electron donor, the length and degree of saturation of the molecular wire, and the intensity of the light were systematically investigated. Optimal conditions included a solution buffered at pH 6.0, cross-linked plastocyanin, rebuilt spinach PS I, and the use of 1,4-benzenedithiol to connect PS I to the Pt nanoparticle. Illumination of this optimized Photosystem I/dithiol molecular wire/nanoparticle bioconjugate at a light intensity of 70 $\mu E\ m^{-2}\ s^{-1}$ generated H_2 at a rate of 312 $\mu mol\ H_2\ mg\ Chl^{-1}\ h^{-1}$ over the course of 24 hours.

The success of these studies has led to the belief that a functional device that utilizes these PS I/molecular wire/nanoparticle bioconjugates could be constructed. Unfortunately, inherent inefficiencies exist within this system due to the use of sacrificial electron donors and the reliance on diffusion chemistry for delivery of electrons to PS I. By directly linking the bioconjugates to an electrode surface, a cathodic half-cell would be created that would be capable of generating H_2 when illuminated. Initial studies have been conducted to look at the interactions between PS I and a gold electrode surface. Ellipsometric measurements and atomic force microscope imaging have revealed that PS I generally maintains its native structure and forms relatively dense monolayers on both –hydroxyl and –carboxyl terminated alkanthiol-capped gold surfaces. This technology could easily be transitioned into a device that incorporates the PS I/molecular wire/nanoparticle bioconjugates for photocatalytic H_2 production.

TABLE OF CONTENTS

LIST OF FIGURES

LIST OF TABLES

ACKNOWLEDGEMENTS

I thank Dr. John Golbeck, my thesis advisor, for all of his assistance and thoughtful scientific discussion throughout my career at The Pennsylvania State University. I thank Dr. Donald Bryant for his scientific guidance. I also thank members of the Golbeck and Bryant labs for their advice that has facilitated my research endeavors. I would like to thank the members of my Thesis Committee for their scientific guidance and suggestions.

I would like to thank my family for their continued support throughout my academic career, especially my parents, Patrick and Rose Grimme, who have assisted me in innumerable ways. They have been a source of inspiration for me to always keep my standards high and my goals in sight. I would like to thank my grandmother, the late Mrs. Mary R. Bearer, for her many years of kind encouragement and guidance. I also thank my best friends Lisa Cione, Julie McCauley, and Becky (Vauthier) Dugan for their friendship, and all of the hysterial laughter and late nights at the bar that have helped me to keep my sanity.

I would like to thank Dr. Miguel A. De la Rosa and Dr. Ming Tien for the gracious gifts of the cytochrome c_6 (*petJ*) expression plasmid and the pEC86 plasmid, respectively. I also thank the Huck Institutes of the Life Sciences Electron Microscopy Facility for the imaging of the Pt and Au nanoparticle samples. I would also thank Dr. James D. Kubicki for performing DFT calculations to determine the length of the molecular wires.

This publication was supported by the Pennsylvania State University Materials Research Institute Nano Fabrication Network and the National Science Foundation Cooperative Agreement No. 0335765, National Nanotechnology Infrastructure Network, with Cornell University. Any opinions, findings, and conclusions or recommendations expressed in this publication are those of the author and do not necessarily reflect the views of Cornell University nor those of the National Science Foundation.

Funding for this research has been provided by the Department of Energy (DE-FG-05-05-ER46222).

Chapter 1

Introduction

An economy based on hydrogen has long been touted as one of the most promising routes to a sustainable energy future. Hydrogen gas (H_2) is a particularly clean source of energy that can be utilized efficiently in hydrogen-based fuel cells. Because the product of energy conversion is H_2O, the use of H_2 does not exacerbate the already existing problem of CO_2 accumulation that is a major component of global climate change. Despite its desirable attributes, H_2 is not found in nature and methods must be employed to generate it using other sources of energy.

Commercial Methods of Hydrogen Production

Commercial methods of producing hydrogen are expensive. These processes include the electrolysis of water and steam reforming of methane. The generation of hydrogen from the electrolysis of water takes place in an electrolytic cell where an electrical power source is connected to a cathode and to an anode, each in separate vessels connected via a salt bridge. The negatively charged electrode combines electrons with protons, and this is where hydrogen is produced. The electrolysis of water requires a larger input of energy than would otherwise be necessary due to the fact that 100% of the electrical power put into the cell is not converted into the chemical bond energy of hydrogen.[1] Steam reforming of methane is less expensive than the electrolysis of water and is therefore the preferred industrial method of production. The heating of steam and methane to high temperatures in the presence of a nickel catalyst results in the generation of H_2 and CO. The further reaction of H_2O and CO produces additional H_2 and CO_2. The by-product of the reaction, CO_2, however, adds to the problem of climate change. Also, because energy is lost by the conversion of methane into hydrogen, it makes little sense to use

one perfectly good fuel to generate another.

With all of the drawbacks associated with currently utilized methods of hydrogen production, researchers are increasingly looking to sunlight as a means of supplying the necessary energy input. Sunlight is abundant, widely distributed, and virtually inexhaustible. The amount of solar energy that strikes the surface of the earth in one hour is more than sufficient to satisfy the total global demand for energy in an entire year.[2] Hence, the photocatalytic production of hydrogen is emerging as an attractive route to the generation of a renewable source of fuel.

Emerging Technologies

A large amount of research has focused on the generation of H_2 by systems that employ gold or platinum nanoparticles supported on semiconductor surfaces such as TiO_2 or Al_2O_3.[3-6] These semiconductor systems function by absorbing a photon and creating an electron-hole pair. The electron migrates to the Au or Pt nanoparticles that are located on the semiconductor surface. These nanoparticles catalyze hydrogen production. A major drawback to this type of system lies in the fact that the band gap of TiO_2 and Al_2O_3 semiconductors is large, and photons with sufficient energy to generate the electron-hole pair can be found only in ultraviolet (UV) radiation.[6] UV, which is light with wavelengths between 200 and 400 nm, constitutes only a small percentage of the solar radiation that reaches the surface of the earth. In an attempt to overcome the band-gap limitation, organic dyes can be introduced into these semiconductor systems to increase the absorption of solar radiation.[3-5] These dyes absorb photons in the visible portion of solar radiation and are thus able to inject electrons directly into the conduction band of the semiconductor materials.[4,5] Once electrons are in the conduction band, they migrate to the Au or Pt nanoparticles loaded on the surface, thereby enabling hydrogen production. While these dye sensitized systems increase the functional working wavelengths that are capable of sustaining the

charge-separated state necessary for hydrogen production, organic dyes are degraded by illumination and moisture, limiting the usefulness of these devices.

Biological and Biohybrid Systems for Light-driven Hydrogen Production

While the dye-sensitized and semiconductor-supported nanoparticle systems hold promise, newer investigations have focused on using both biological systems and biohybrid designs to photocatalytically generate H_2. It is generally accepted that any photocatalytic system for generating a usable fuel from sunlight will require three components: a module that converts sunlight into an electric current, a module that catalyzes the reduction of protons to H_2, and a linker that facilitates the transfer of electrons from the light module to the catalytic module.

In Vivo Systems Produce Hydrogen

In vivo systems couple Photosystem I (PS I), naturally occurring light harvesting complexs, to hydrogen evolving catalysts. The advantages of utilizing PS I as the energy-converting module are discussed in detail below. *In vivo* experiments using photosynthetic organisms have shown that hydrogen can be evolved by the enzymes nitrogenase (N_2ase) and hydrogenase (H_2ase).[7,8] Hydrogen is produced as a byproduct of nitrogen fixation by N_2ase and it is a natural product of H_2ase when an electron donor is present.[7] When the reducing equivalents from PS I are directed to H_2ases or N_2ases (the linker being a redox protein), cyanobacteria and microalgae evolve hydrogen.[8] A major drawback to these *in vivo* systems is that the efficiency of hydrogen generation will always be limited due to the amount of solar energy necessary to sustain the growth and metabolism of the organism. A further drawback is that N_2ases and H_2ases are oxygen sensitive, making hydrogen generation problematic in the presence of oxygenic

photosynthesis.

Photosystem I Fusion Systems

In vitro systems that combine biological and/or non-biological components in novel ways were the first attempt at a hybrid approach for hydrogen production. These *in vitro* systems utilize isolated proteins or proteins within chloroplasts in conjunction with metal deposition and/or naturally occurring H_2ases. A PS I-H_2ase construct has been created by fusing the gene encoding for the [NiFe]-H_2ase from *Ralstonia eutropha* H16 with the gene encoding the PsaE (PS I stromal) protein. When the H_2ase/PsaE fusion product is re-bound to a PsaE deletion mutant of PS I, hydrogen is evolved, albeit at low rates (0.2 μmol H_2 mg Chl^{-1} h^{-1}).[9] A further study cross-linked cytochrome c_3 (cyt c_3) from *Desulfovibrio vulgaris*, which is the natural electron donor to the *D. vulgaris* periplasmic [FeFe]-hydrogenase, to PsaE.[10] The cross-linking was carried out on variants in which a Cys residue was introduced at position 4 of cyt c_3 and a Lys residue was introduced at position 40 of PsaE. Cross-linking was achieved using the heterofunctional cross-linker N-[4-maleimidobutyryloxy]sulfosuccinimide which reacts both with primary amines and thiol groups. The cyt c_3/PsaE complex was rebound to a PsaE deletion mutant of PS I and was introduced to a solution containing the *D. vulgaris* [FeFe]-hydrogenase enzyme. When illuminated, light-induced H_2 generation was observed at a maximum rate of 0.56 μmol H_2 mg Chl^{-1} h^{-1}.[10]

Platinized Chloroplasts

The Hill reaction of photosynthesis, which reduces ferric ions to ferrous ions, forms the basis for the photoprecipitation of metallic platinum onto the external surfaces of spinach

thylakoid membranes and isolated Photosystem I protein complexes in work completed by Greenbaum and coworkers.[11-13] Initial experiments precipitated Pt onto chloroplasts by incubation with H_2 and subsequent isolation of the platinized chloroplasts, followed by illumination.[11] Both H_2 and O_2 are evolved simultaneously by illuminating these pre-platinized chloroplasts as O_2 is evolved from PS II that is present in the thylakoid membranes, and H_2 is evolved from the precipitated colloidal Pt.[12] In further experiments, electrons supplied by PS I act as the reductant for the platinum precipitation.[13] When hexachloroplantinate ($[PtCl_6]^{-2}$) is added to a solution containing spinach chloroplasts, and the solution is illuminated, PS I supplies 4 electrons and the Pt ion is reduced to Pt(s).[12] Once the Pt has precipitated onto the chloroplasts, continued illumination was shown to enable H_2 production. Maximum H_2 production was observed in colloids that averaged between 50 and 500 Pt atoms.[12] Hexachloroosmiate ($[OsCl_6]^{-2}$) can also be photoprecipitated onto chloroplasts and is capapble of photocatalytic H_2 evolution, and at faster rates than that of the platinized chloroplasts.[13] Additionally, hexachlororuthenate $[RuCl_6]^{-2}$ can be photoprecipitated onto chloroplasts alone or in combination with $[PtCl_6]^{-2}$ and is also capable of evolving H_2 and the precipitated colloids have been imaged by both SEM and AFM.[14]

Platinized Photosystem I

The orientation of PS I within thylakoid membranes, with the reducing equivalents being produced on the external side of the membrane, enabled the direct photoprecipitation of metallic platinum on spinach PS I within the membranes. Isolated PS I protein complexes have also shown the ability to have Pt photoprecipitated onto their stromal interfaces.[15] The method for the photoprecipitation of isolated spinach PS I included the introduction of plastocyanin (Pc) which is the native electron-donating species to spinach PS I. Pc was introduced to supply electrons to PS

I that are necessary for the photoreduction of $[PtCl_6]^{-2}$. Additionally, it was shown that Pc was necessary for the rapid re-reduction of PS I for H_2 evolution by a series of sequential addition control experiments.[15] The cross-linking of Pc to spinach PS I , followed by platinization and illumination enabled H_2 production at a rate twice that of the non-cross-linked sample.[16]

Efficient Photon Capture and Energy Conversion by Photosystem I

PS I is a light harvesting complex that is located in the photosynthetic membranes of plants and cyanobacteria, a photosynthetically active bacteria. The major purpose of PS I is to use the energy of light to transfer electrons from high potential (i.e. low energy) redox proteins across the membrane to low potential (i.e. high energy) redox proteins.[17] **Figure 1-1** depicts the arrangement of PS I proteins within the membrane. Although PS I comprises 13 proteins, PsaA, PsaB, and PsaC are of the most interest. PsaA and PsaB are intramembrane proteins which support the core electron transfer cofactors of PS I, while PsaC lies outside of the membrane and acts as an interface to shuttle electrons from within the membrane to soluble low potential electron accepting proteins. **Figure 1-2** affords a more detailed look at the organization of PS I. Additional intramembrane proteins surround the PsaA/PsaB heterodimer and support ~100 antenna chlorophyll molecules that are active in ligh harvesting.[18] These antenna pigments in cyanobacterial PS I are chlorophyll *a* (Chl *a*) molecules that are capable of absorbing photons with wavelengths shorter than 700 nm. This absorbance corresponds to 43-46% of the total solar radiation that reaches the surface of the earth.[19] When a Chl *a* molecule absorbs a photon, an excited state is created; the energy is ultimately transferred by resonance energy transfer to the primary electron donor of PS I, a Chl *a* special pair, termed P700. The arrangement of the core electron transfer cofactors is shown in **Figure 1-3**. When the exciton reaches P700, a charge-separated state occurs between P700 and the primary electron acceptor, A_0, another Chl *a*.

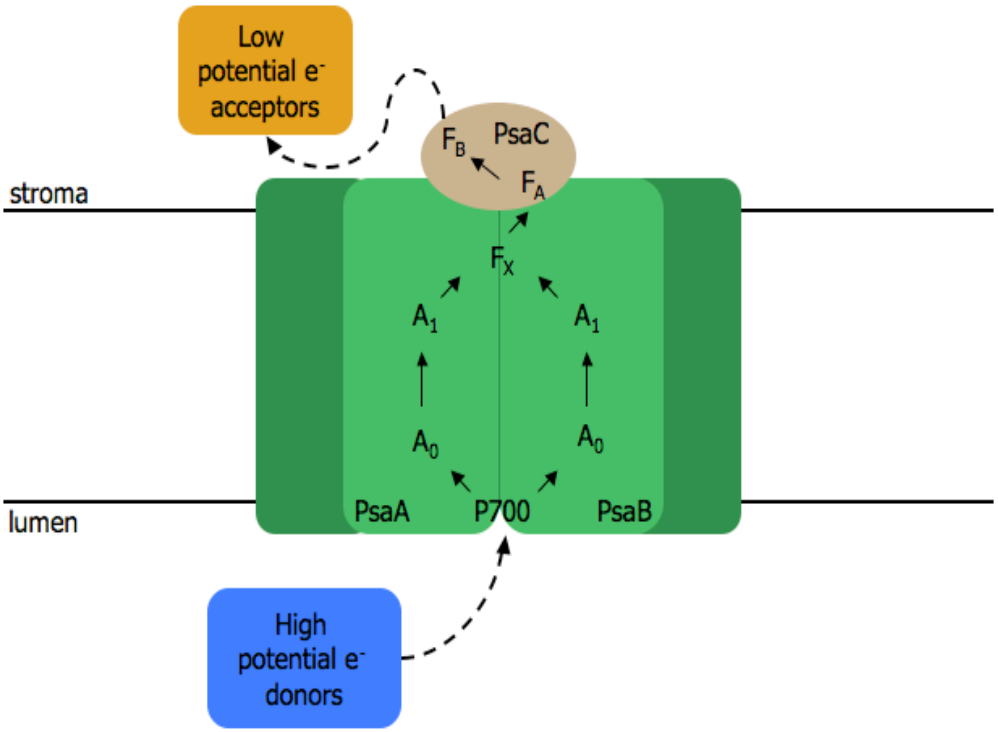

Figure **1-1**: This cartoon depicts Photosystem I within the thylakoid membrane. PsaA and PsaB (light green) are an intramembrane protein heterodimer that contain the core electron transfer cofactors within PS I—P700, A_0, A_1, and F_X. PsaC lays outside of the membrane on the stromal side of PS I and harbors the electron transfer cofactors F_A and F_B. Additional intramembrane proteins (dark green) support antenna chlorophyll molecules that are responsible for light harvesting. High potential (low energy) electron donating proteins (plastocyanin or cytochrome c_6) provide electrons to P700. The light-driven electron transfer through the membrane is photocatalyzed by photons absorbed by the antenna chlorophyll molecules. Electrons ultimately arrive on the stromal side of PS I at F_B and can then transfer to soluble low potential (high energy) electron accepting proteins (ferredoxin or flavodoxin).

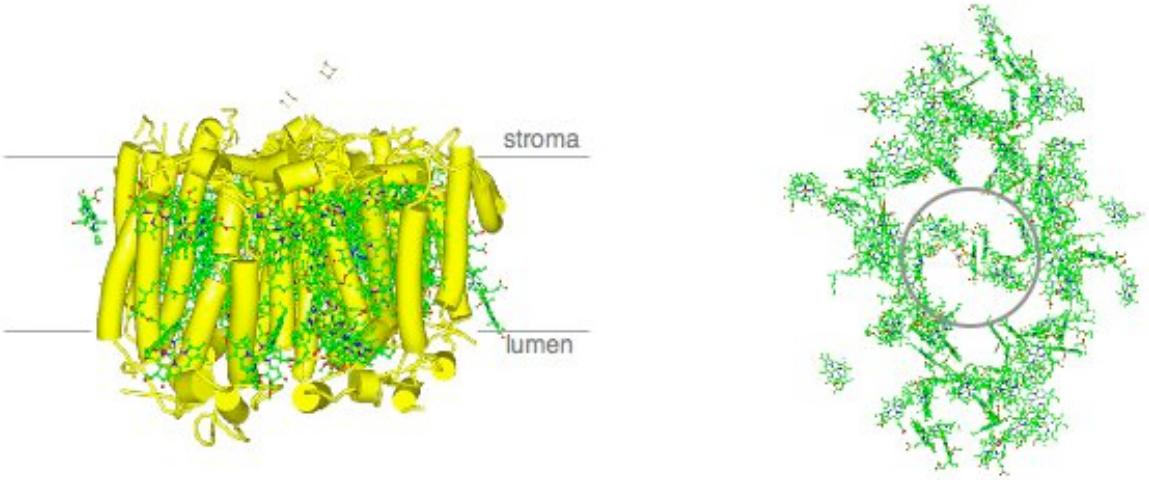

Figure **1-2**: The intramembrane α-helices of PS I (yellow tubes) act as scaffolds for antenna Chl *a* molecules (green) and the core electron transfer cofactors; the [4Fe-4S] clusters, F_A and F_B, are visible on the stromal side (a). Rotating structure (a) 180° and removing the protein scaffold affords a look (top down from the stromal side) at the organization of the antenna Chl *a* molecules around the core electron transfer cofactors (circled in grey) (b).

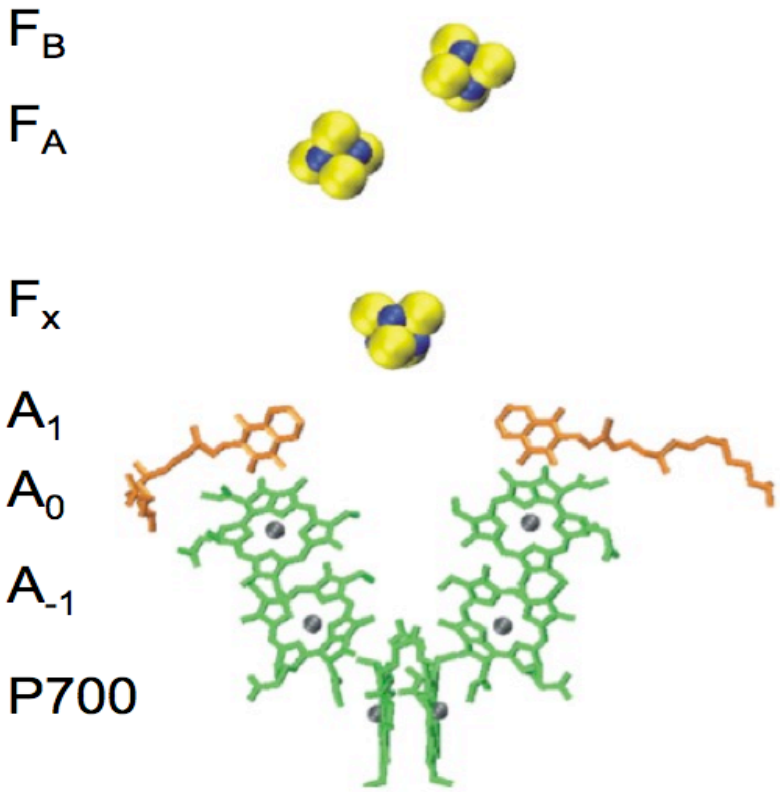

Figure **1-3**: The core electron transfer cofactors are arranged to allow for light-induced electron transfer to occur rapidly from P700, through the cofactors, to F_B. A charge-separated state is first established between P700 and A_0. The electron is then transferred to A_1, a bound phyloquinone molecule, and then to three [4Fe-4S] clusters. The first of these, the inter-polypeptide [4Fe-4S] cluster, F_X, is ligated by cysteine residues provided by both PsaA and PsaB. The stromal protein PsaC harbors the two terminal [4Fe-4S] clusters, F_A and F_B.

Ultimately, the electron is transferred through the other electron transfer cofactors to F_B, the terminal cofactor within PS I. The F_B cluster has a midpoint potential of -580 mV, which is more than sufficient to reduce protons to H_2.[17] The quantum yield of PS I approaches 1.0 which

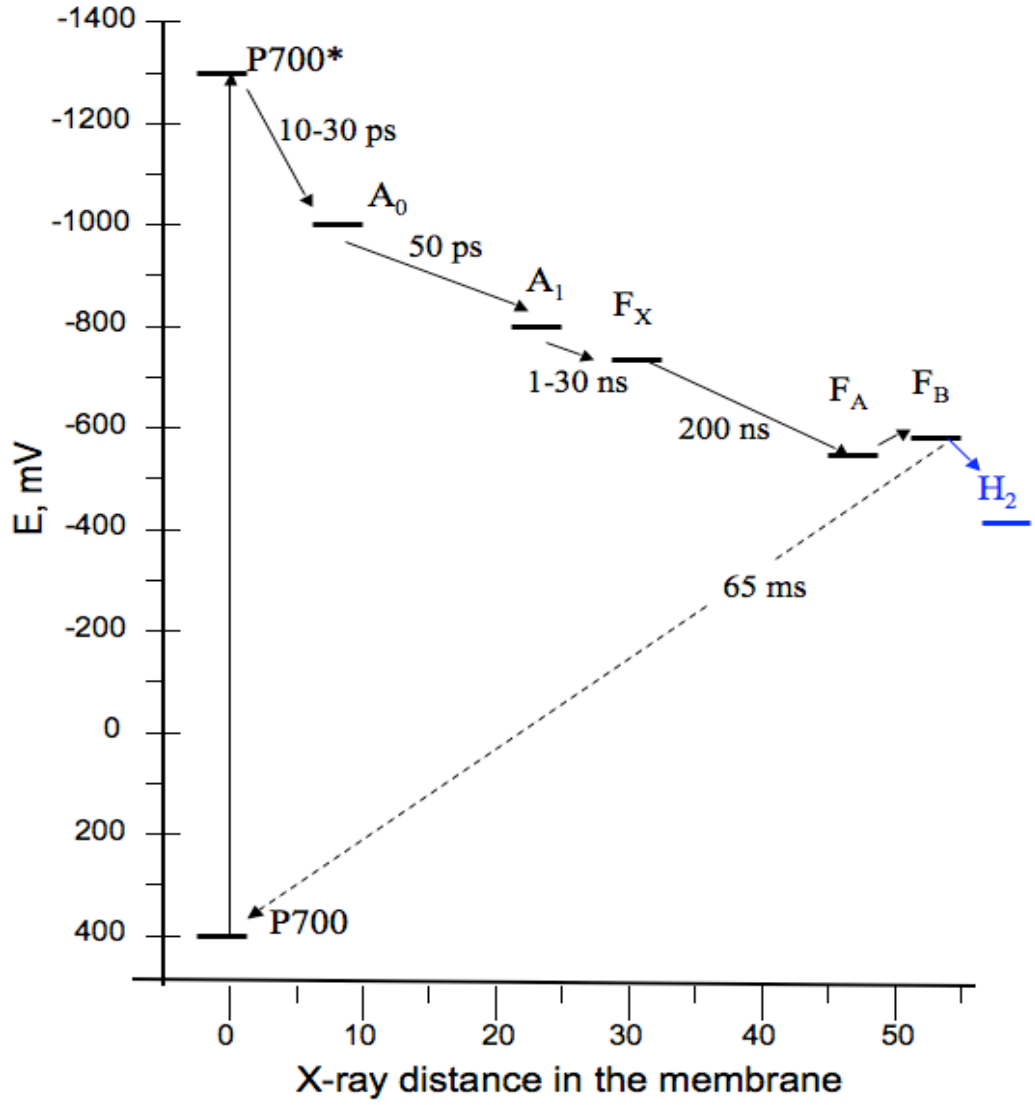

Figure **1-4**: As the electron is transferred away from P700, the potential of the cofactors becomes more positive, thus the transfer is thermodynamically downhill and favorable. Further electron transfer from F_B^- to a H_2 evolving entity (Pt nanoparticle or H_2ase enzyme) is also thermodynamically favorable as the redox potential for H_2 evolution is thermodynamically more positive than that of the F_B cluster.

means that nearly all of the photons that PS I absorbs are converted to the charge separated state $P700^+/F_B^-$.

Electron transfer on the PS I acceptor side is thermodynamically favorable, as the midpoint potential of each of the subsequent cofactors is more positive than the previous one. **Figure 1-4** shows the potentials of the electron transfer cofactors as a function of their distance from P700 as well as forward electron transfer and charge-recombination times. The electron transfer from P700 to F_B is rapid (~200 ns) and the lifetime of the charge-separated state, $P700^+/F_B^-$, is long (~65 ms).[20] Provided the electron is transferred away from the F_B cluster within this lifetime, charge recombination will not occur and electron can be harnessed for useful work. In the case of normal photosynthesis, this work is the reduction of ferredoxin or flavodoxin (and the subsequent production of NADPH), but if the electron can be removed at F_B^- directly, it can be used to reduce protons to H_2.

Hydrogen Catalysis by Platinum Nanoparticles

As in the case of semiconductor systems, Pt nanoparticles can be used as the catalyst for hydrogen generation. H^+ ions adsorb onto the Pt surface and combine with an electron to form an H atom. A covalent bond is catalytically generated between two adsorbed H atoms to yield H_2. H_2 then desorbs from the Pt surface. At pH 7.0, this process occurs at a midpoint potential of -420 mV. If the electrons are derived from the F_B cluster of PS I, there is ~160 mV of thermodynamic driving force for this reaction to occur. This translates to an equilibrium constant greater than 10^2, indicating that this reaction will be a highly favorable reaction on thermodynamic grounds.

In practice, a system could be set up in which PS I and Pt nanoparticles are suspended in solution, however hydrogen generation would most likely be of low yield due to the fact that the

interactions between nanoparticles and PS I would be controlled by slow diffusion chemistry. The speed of diffusion decreases as size of the body in motion increases. In this case, both the PS I and the Pt nanoparticles are large entities and diffusion would likely be too slow to transfer the electron from F_B^- to the nanoparticle surface before the charge recombination between $P700^+$ and F_B^- would occur. In order to avoid this inevitable loss of energy, a direct link should be made between the PS I and the Pt nanoparticle.

Molecular Wires Form a Covalent Pathway

Molecular wires are the answer to the diffusional limitation in electron transfer. A molecular wire, in the form of an aliphatic or aromatic hydrocarbon chain, can be used to connect PS I with the Pt nanoparticle. On one hand, the molecular wire should be sufficiently long to shield the protein from the nanoparticle surface to limit protein denaturation. On the other hand, the molecular wire should be sufficiently short enough to allow for efficient energy transfer between the two modules. Because the charge-separated state $P700^+/F_B^-$ is stable for ~65 ms, efficient electron transfer away from F_B must occur on the order of 1 ms. Marcus theory, which relates the rate of electron transfer to the distance between the cofactors (as well as the Gibbs free energy change, reorganization energy, and temperature), governs the maximum distance between PS I and the Pt nanoparticle for optimal electron transfer. Under ideal conditions, for the electron to be transferred on the microsecond timescale, the distance between the cofactors should be shorter than 2.0 nm. Short aliphatic and aromatic hydrocarbons with thiol moieties easily functionalize Pt nanoparticle surfaces and are commercially available. Unfortunately, a direct bond cannot be made to native PS I without modification.

Manipulation of Photosystem I

In order to attach the molecular wire, a variant of the PsaC subunit was engineered in which the native cysteine ligand to the F_B cluster at position 13 is replaced with a glycine residue in the C13G/C33S variant. Glycine lacks a side chain, and is hence incapable of ligating the Fe atom. However, its use opens up a site to which a molecular wire can be attached. The iron-free form of the PsaC variant is expressed in *Escherichia coli* and the F_A and F_B clusters are inserted using inorganic [4Fe-4S] clusters ligated by 2-mercaptoethanol. The PsaC variant can then be re-bound to previously prepared PS I cores that lack the PsaC subunit. Analytical techniques show that two [4Fe-4S] clusters are inserted into the protein despite the absence of one of the cysteine ligands to F_B. This anomaly has been explained by the fact that the [4Fe-4S] clusters are inserted into the protein *in vitro* by a ligand exchange mechanism in which the 2-mercaptoethanol ligands are displaced by the protein cysteine ligands. At the glycine position, the 2-mercaptoethanol is retained, where it functions as a so-called rescue ligand for the F_B cluster. The insertion process, incidentally, is driven to completion by the entropic gain realized when seven 2-mercaptoethanol molecules are released into solution during the insertion process. Thiol functionalities in the form of a molecular wire can then readily displace the single 2-mercaptoethanol ligand through facile sulfur-iron displacement reactions.[21,22]

Catalytic Hydrogen Production Using Bioconjugates

Bioconjugates composed of Photosystem I, a molecular wire, and gold or platinum nanoparticles can be prepared using this thiol-displacement strategy. When utilizing a dithiol molecule as the molecular wire, one functional group of the thiol acts to displace the 2-mercaptoethanol ligand from the F_B cluster while the other functional group serves to

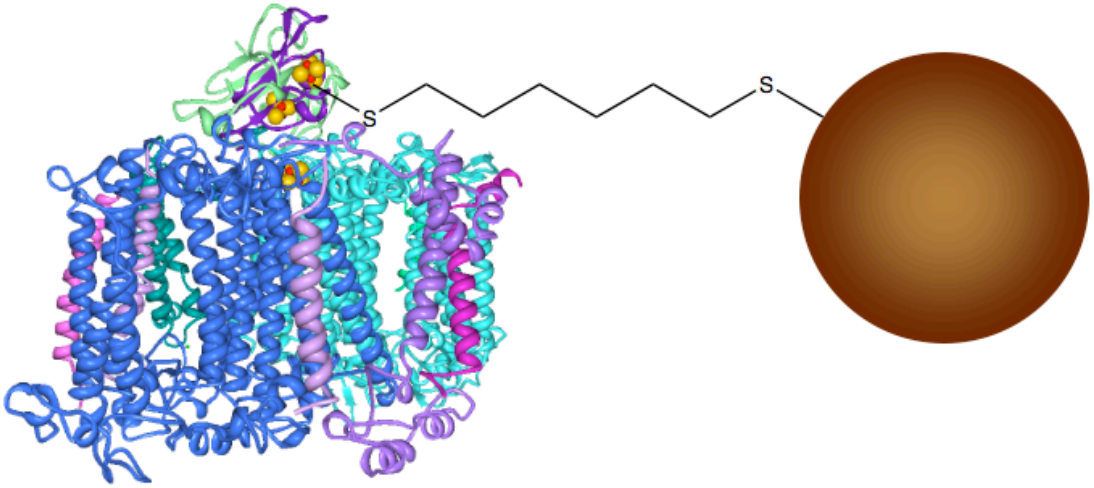

Figure **1-5**: This bioconjugate is composed of Photosystem I rebuilt from recombinantly expressed C13G/C33S variant PsaC, PsaD, and P700/F_X cores,a 1,6-hexanedithiol molecular wire, and either Au or Pt nanoparticles. The molecular wires serves not only as a covalent link between PS I and the nanoparticle but also acts as a conduit for electron transfer. The electron donor, cytochrome c_6, is not depicted here.

functionalize the nanoparticle surface. Providing an electron donating species and an illumination source enables H_2 production.

Establishing Hydrogen Production

A bioconjugate composed of rebuilt cyanobacterial PS I containing the glycine variant of PsaC, 1,6-hexanedithiol molecular wires, and either 12 nm Au or 3 nm Pt nanoparticles was assembled as shown in **Figure 1-5**. Sodium ascorbate serves as the sacrificial electron donor to dicholorophenylindophenol (DCPIP), which donates electrons directly to $P700^+$. When the system is illuminated, H_2 was generated at low rates over a period of 24 hours. The addition of

cytochrome c_6, which is a superior electron donor to $P700^+$, resulted in hydrogen generation at higher rates.[23] These studies are described in detail in Chapter 2.

Maximizing Hydrogen Production

While the initial rates for this system were already promising, continued research yielded better performance. In iterative studies, using spinach PS I rebuilt with the C13G/C33S variant of PsaC, altering the pH and the ionic strength of the solution, changing the length and the aromaticity of the molecular wire, as well as cross-linking plastocyanin to the rebuilt PS I was shown to increase the rate of hydrogen generation by the PS I/molecular wire/Pt nanoparticle bioconjugates.[24] These studies are discussed in Chapter 3.

Moving Toward Functional Devices

These initial studies have provided solid evidence that a PS I-based biohybrid system has potential to be used in a H_2 producing device. However, a major drawback to these studies lies in the aqueous solution-based nature of the systems that relies on inefficient diffusion chemistry and sacrificial-electron donating species. To establish a functional device, these drawbacks should be eliminated or dimished. One method to eliminate diffusion chemistry and the need for sacrificial electron-donating species would be to directly link PS I to an electrode surface. Chapter 4 examines at the strategies for functionalizing electrode surfaces with PS I and discusses initial results for attaching PS I to electrode surfaces.

Summary

The ability to photocatalytically generate clean hydrogen fuel has the potential to satisfy the global demand for storable energy and has advantages over the costly and environmentally unfriendly current means of hydrogen production. Biological systems have advantage over semiconductor-supported Au and Pt nanoparticle systems in their ability to absorb a broad spectrum of solar radiation. Biologically inspired systems that employ PS I as a means of photon capture and as a source of reducing electrons are yielding promising results in solar energy conversion to hydrogen production. When PS I is attached to nanoparticles, the light-driven generation of hydrogen is observed. Further studies to directly attach this system to electrode surfaces may lead to a functional device.

References

1. Rosen, M.A., Scott, D.S., *Int. J. Hydrogen Energy*, **1998**, *23*, 653.
2. United Nations Development Program, *World Energy Assesment Report: Energy and the Challenge of Sustainablity*, **2003**, United Nations, New York.
3. Mizukoshi, Y., Makise, Y., Shuto, T., Hu, J., Tominaga, A., Shironita, S., Tanabe, S., *Ultrasonics Sonochem.*, **2007**, *14*, 387.
4. Gurunathan, K., Maruthamuthu, P., Sastri, M.V.C., *Int. J. Hydrogen Energy*, **1997**, *22*, 57.
5. Dhanalakshmi, K.B., Latha, S., Anandan, S., Maruthamuthu, P., *Int. J. Hydrogen Energy*, **2001**, *26*, 669.
6. Tang, H., Berger, H., Schmid, P.E., Levy, F., *Solid State Commun.*, **1994**, *92*, 267.
7. Melis, A., Zhang, I., Forestier, M., Ghirardi, M.L., Seibert, M., *Plant Physiol.*, **2000**, *122*,

515.

8. Schutz, K., Happe, T., Troshina, O., Lindblad, P., Leitao, E., Oliveira, P., Tamagnini, P., *Planta*, **2004**, *218*, 350.

9. Ihara, M., Nishihara, H., Yoon, K.S., Lenz, O., Friedrich, B., Nakamoto, H., Kojima, K., Honma, D., Kamachi, T., Okura, I., *Photochem. Photobioil.*, **2006**, *82*, 676.

10. Ihara, M., Nakamoto, H., Kamichi, T., Okura, I., Maeda, M., *Photochem. Photobiol.*, **2006**, *82*, 1677-1685.

11. Greenbaum, E., *Science*, 1985, **230**, 1373-1375.

12. E. Greenbaum, *J. Phys. Chem.*, 1988, **92**, 4571-4574.

13. J. W. Lee, C. V. Tevault, S. L. Blankinship, R. T. Collins and E. Greenbaum, *Energ. Fuel.*, 1994, **8**, 770-773.

14. J. W. Lee, I. Lee and E. Greenbaum, *J. Phys. Chem. B*, 2005, **109**, 5409-5413.

15. J. F. Millsaps, B. D. Bruce, J. W. Lee and E. Greenbaum, *Photochem. Photobiol.*, 2001, **73**, 630-635.

16. B. R. Evans, H. M. O'Neill, S. A. Hutchens, B. D. Bruce and E. Greenbaum, *Nano Lett.*, 2004, **4**, 1815-1819.

17. Brettel, K., *Bichim. Biophys. Acta*, **1997**, *1318*, 322.

18. Jordan, P., Fromme, P., Witt, H.T., Klukas, O., Saenger, W., Krauss, N., *Nature*, **2001**, *411*, 909.

19. Gibbs, M., Holaender, A., Kok, B., Krampitz, L.O., San Pietro, A., A report on a workshop held September 5-6, 1973, at Bethesda, MD, supported by NSF under RANN Grant GI 40253 to Indiana University.

20. Shinkarev, V.P., Vassiliev, I.R., Golbeck, J.H., *Biophys. J.*, **2000**, *78*, 363.

21. Antonkine, M.L., Maes, E.M., Czemuszewiez, R.S., Breitenstein, C., Bill, E., Falzone, C.J., Balasumbramanian, R., Lubner, C.E., Bryant, D.A., Golbeck, J.H., *Biochim.*

Biophys. Acta, **2007**, *1767*, 712.

22. Que, L. Jr., Bobrik, M.A., Ibers, J.A., Holm, R.H., *J. Am. Chem. Soc.*, **1974**, *96*, 4168.

23. Grimme, R.A., Lubner, C.E., Bryant, D.A., Golbeck, J.H., *J. Am. Chem. Soc.*, **2008**, *130*, 6308-6309.

24. Grimme, R.A., Lubner, C.E., Golbeck, J.H., *Dalton Transactions*, **2009**, submitted.

Chapter 2

Photosystem I/Molecular Wire/Metal Nanoparticle Bioconjugates for the Photocatalytic Production of H_2*

Introduction

In recent years, gold and platinum nanoparticles have become attractive platforms for the photocatalytic production of hydrogen gas.[1,2] Photocatalysis of H_2 has been achieved by means of alcohol reforming on the surface of Au and Pt nanoparticles supported on semiconductor materials such as titania.[3–6] These semiconductor materials supply an input of energy in the form of electrons. A major drawback to this type of H_2 photocatalysis is that the photons must have an energy greater than the band gap of the semiconductor material in order to produce a charge-separated state that is able to sustain the reaction: $2H^+ + 2e^- \rightarrow H_2$. For titania, the band gap is ~3.2 eV and corresponds to light with wavelengths shorter than ~350 nm.[7] On the basis of this requirement, only a very small fraction of incident solar radiation has sufficient energy to produce this state. The photosynthetic complex, Photosystem I (PS I), produces a light-induced, charge-separated state that could be used to generate reducing equivalents for H_2 production. The covalent attachment of PS I to Au and Pt nanoparticles provides an attractive alternative to the titania-supported particles for the photocatalytic production of H_2.

PS I has highly favorable properties that favor its use in such applications. The pigments that comprise the antenna complex of PS I absorb all wavelengths of visible light shorter than ~700 nm, which represents 43-46% of the total solar radiation that reaches the surface of the

* Reproduced with full permission from "Grimme, R.A., Lubner, C.E., Bryant, D.A., Golbeck, J.H., *J. Am. Chem. Soc.*, **2008**, *130*, 6308-6309." Copyright 2008 American Chemical Society.

earth.[8] PS I has a quantum yield that approaches 1.0; hence nearly all of the photons that are absorbed are converted into the charge-separated state $P700^+/F_B^-$. This charge-separated state is stable for ~100 ms, and the low potential reductant that is produced is poised at a redox potential favorable for H_2 evolution.

The challenge is to transfer the electron from PS I to the nanoparticle surface within this 100 ms time frame. We describe the covalent linkage between PS I and gold or platinum nanoparticles via a molecular wire which enables electron transfer and subsequent H_2 production.

A covalent link between the nanoparticle and the terminal electron transfer cofactor of PS I, F_B, can be fabricated. Recent work in our laboratory highlights the ability of the C13G/C33S variant of PsaC that lacks a native cysteine ligand at a solvent-exposed position on the F_B cluster to be chemically rescued by a thiolated organic molecule.[9] This PsaC variant has the unique ability to transfer electrons from the F_B cluster to a covalently bound external acceptor. The functionalization of Au and Pt surfaces by thiolated molecules is an extensively explored and well-documented field of study.[10–14] It was therefore considered feasible to link Au and Pt nanoparticles covalently to PS I via a bifunctional organic dithiol which serves as the molecular wire.

Materials and Methods

Materials

H_2O used for all experiments was doubly distilled. All chemicals were purchased from commercial suppliers (Sigma Aldrich and VWR Scientific) and were used without further purification.

Instrumentation

Transmission Electron Microscope (TEM) imaging was obtained using a JEOL-JEM 1200 EXII microscope operating at 80 keV and images were captured on a Gatan Bioscan 792 digital camera. UV/Visible spectroscopic analysis was performed using a Varian Carry Bio 50 UV/Visible spectrophotometer. Gas chromatography (GC) analyses were performed using a Shimadzu GC-8A gas chromatograph equipped with a thermal conductivity detector. For all GC analyses, the column was a packed ShinCarbon ST 80/100 column (2m x 2 mm). The carrier gas was ultra-pure N_2 and had a flow rate of 0.75 mL/min. Injection port/detector temperature was 100 °C and colum temperature was maintained at 40 °C. Detector current was set at 100 mA.

Nanoparticle Synthesis

Aqueous synthesis of 12 nm Au and 3 nm Pt nanoparticles was carried out according to literature procedures.[15,16] The size of the resulting particles was found to be 12.37 ± 1.12 nm for the citrate-stabilized Au nanoparticles (Figure 1-1-a) and 2.89 ± 0.41 nm for the mercaptosuccinic acidstabilized Pt nanoparticles (Figure 1-1-b) by TEM analysis.

Protein Purification

Photosystem I was purified using standard literature procedures from *Synechococcus* sp. PCC 7002 grown in A_+ medium to an optical density of 0.8.[17] PsaD from *Synechococcus* sp. PCC 7002 was overproduced in *Escherichia coli* BL21 (DE3) cells and was purified using standard literature procedures.[18] The C13G/C33S variant of PsaC from *Synechococcus* sp. PCC 7002 was overproduced in *E. coli* BL21 (DE3) cells and was purified using previously published methods.[19]

Cytochrome c_6 from *Synechocystis* sp. PCC 6803 was overproduced in *E. coli* BL21 (DE3) cells and was purified according to standard literature procedures.[20] Protein concentrations were determined by UV/Visible spectroscopy, and protein purity was assessed by SDS-PAGE. All proteins were stored at -80 °C after purification unless otherwise specified.

P700/F_X Core Preparation

Purified PS I was subjected to 9 M urea to remove the native stromal proteins PsaC, PsaD, and PsaE following a procedure similar to those previously published.[21,22] Stromal protein removal was monitored by observing a decrease in the amplitude of the kineic phase that corresponds to the charge recombination between F_B^- and $P700^+$ using flash-induced optical spectroscopy (data not shown).

In Vitro Reconstitution of C13G/C33S Variant PsaC

Fe-S clusters constructed from Na_2S, $Fe(NH_4)_2(SO_4)_2^{2+}$, and 2-mercaptoethanol under anaerobic conditions and inserted into the apo-C13G/C33S variant of PsaC by a ligand exchange mechanism.[23] Insertion of the clusters was verified by EPR spectroscopy and by iron and acid-labile sulfide analysis (data not shown).[24,25] The holo-C13G/C33S variant of PsaC was stored under liquid N_2 and handled anaerobically to prevent cluster degradation.

Reassembly of Photosystem I

PS I was reassembled by combining P700/Fx cores with the holo-C13G/C33S variant of PsaC, and PsaD at a ratio of 1:500:50, respectively.[18] PS I was allowed to assemble overnight

under anaerobic conditions and was then concentrated by ultrafiltration over a 30 kDa-cutoff filter to remove unbound C13G/C33S variant PsaC and PsaD.

Photosystem I/Molecular Wire/Nanoparticle Bioconjugate Formation

PS I/nanoparticle bioconjugates were prepared by combining assembled PS I complexes (5 μM Chl, 5.8 nM PS I final concentration) with either Au or Pt nanoparticles and 1,6-hexanedithiol (200 nM final concentration) and were allowed to assemble in the dark for ~2 hours while under slight agitation. Controls were treated in the same manner as the experimental group, but lacked one or more of the system components. Dichlorophenylindophenol (DCPIP), Na-ascorbate, and Cyt c_6 (final concentrations of 10 μM, 100 mM, and 5 μM, respectively) were added to appropriate samples before addition to N_2 purged vials.

H_2 Evolution Studies

Following addition to N_2 purged vials, unless otherwise noted, samples were illuminated by a xenon arc lamp (after passage through a water filter to remove the IR and UV portions of the illuminating radiation and to maintain the temperature of the reactions between 20 and 22 °C) and H_2 production was evaluated every 4 hours by GC analysis of 200 μL headspace gas samples. Rebuilt PS I/1,6-hexane dithiol/Au and rebuilt PS I/1,6-hexane dithiol/Pt nanoparticle bioconjugates produced H_2 while illuminated continuously for 12-16 hours.

Results and Discussion

One functional group of the dithiol molecule modified the surface of the nanoparticle, while the other functional group served as the rescue ligand to the F_B cluster. Due to its relatively short length (~1.2 nm), which enables electron transfer from PS I to the nanoparticle before the otherwise inevitable charge recombination between $P700^+$ and F_B occurs, 1,6-hexanedithiol was chosen as a molecular wire for these experiments.

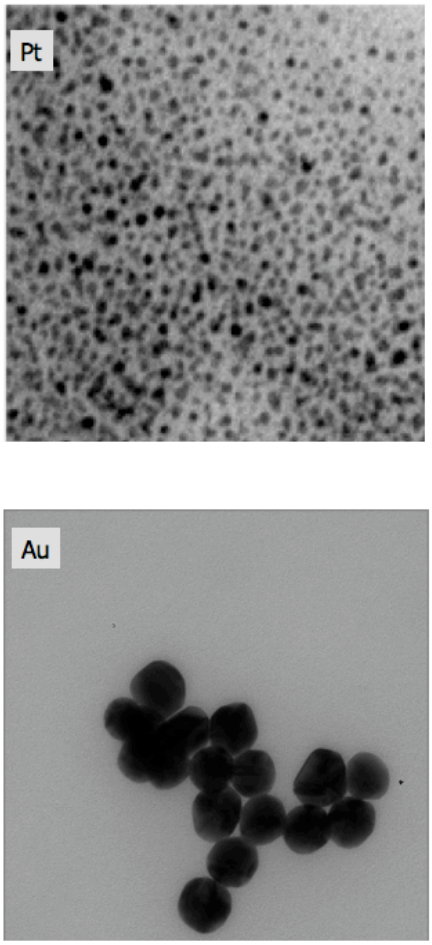

Figure **2-1**: Typical TEM images of 3 nm Pt (a) and 12 nm Au (b) nanoparticles.

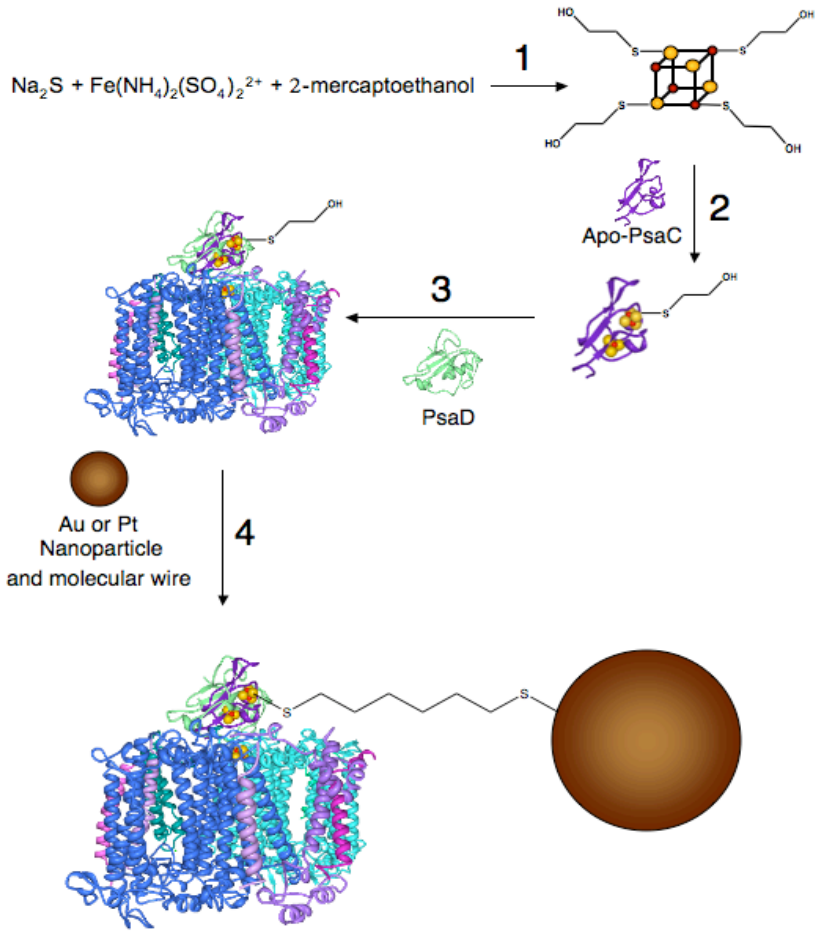

Figure **2-2**: Construction of the Photosystem I/1,6-hexanedithiol/nanoparticle bioconjugatebegan with the formation of [4Fe-4S] clusters in solution by combining sodium sulfide, ferrous ammonium sulfate, and 2-mercaptoethanol (1). Apo-C13G/C33S variant PsaC was reconstituted in vitro with these [4Fe-4S] clusters (2) to yield holo-C13G/C33S variant PsaC. PS I was rebuilt by combining reconstituted PsaC and P700/F_X cores in the presence of PsaD (3). The 2-mercaptoethanol ligand to the F_B cluster was displaced, and PS I was covalently linked to a Pt or Au nanoparticle by 1,6- hexanedithiol (4).

For all experiments, nanoparticles were synthesized according to previously published methods. As determined by TEM analysis of 224 and 208 particles, respectively, these methods resulted in 12.37 (1.12 nm citrate stabilized Au nanoparticles or 2.89 (0.41 nm mercaptosuccinic acid stabilized Pt nanoparticles (Figure 2-1).[15,16] The iron-sulfur clusters in the C13G/C33S variant of PsaC were reconstituted with ferrous ammonium sulfate, sodium sulfide, and 2-mercaptoethanol, which resulted in its rebinding to P700/F_X cores in the presence of PsaD (Figure 2-2, 1-3). The rebuilt PS I was then introduced into solutions containing either 12 nm Au nanoparticles or 3 nm Pt nanoparticles at a ratio of 1:1 PS I/nanoparticle (Figure 2-2, 4). The final concentration of PS I was 5.0 μg/mL Chl *a* (5.8 nM PS I). 1,6-Hexanedithiol was added to a final concentra- tion of 200 nM to displace the 2-mercaptoethanol ligand that had been retained at the open coordination site of the F_B cluster and to link PS I to the nanoparticle surface. Samples were treated in the dark for ~2 h with slight agitation, which allowed the PS I/nanoparticle bioconjugates to assemble. Dicholoro(phenol)indophenol (DCPIP), at 10 μM final concentration, which was reduced by the sacrificial donor sodium ascorbate, at a concentration of 100mM, served as the electron donor to $P700^+$. To evaluate whether the reaction was donor-side limited, cytochrome c_6 (Cyt c_6) was added to a PS I/molecular wire/Pt nanoparticle bioconjugate sample due to the fact that Cyt c_6 is a much faster donor to $P700^+$ than is reduced DCPIP.

The PS I/nanoparticle bioconjugates were added to closed vessels with a path length of 2.0 cm that had been purged with N_2 gas, and the samples were illuminated continuously with saturating white light from a Xenon arc lamp at an intensity of 2500 μE for 12-16 hours. Samples were taken from the headspace gas every 4 hours and were analyzed for H_2 by gas chromatography (Figure 2-3). Both PS I/molecular wire/Au nanoparticle and PS I/molecular wire/Pt nanoparticle bioconjugates were able to produce H_2 upon illumination (Table 2-1). PS I/molecular wire/Au nanoparticle bioconjugates generated 3.4 μmol H_2 mg Chl^{-1} h^{-1}, while PS

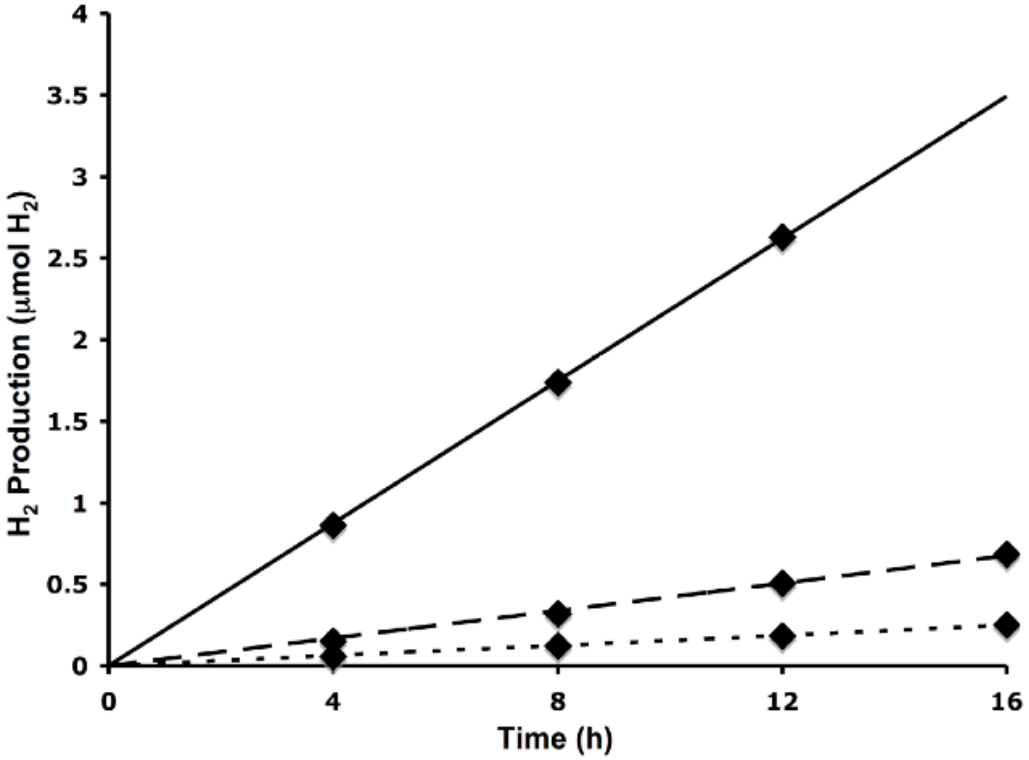

Figure **2-3**: Hydrogen production is observed for PS I/1,6-hexanedithiol/Au nanoparticle bioconjugates without Cyt c_6 (…) and PS I/1,6-hexanedithiol/Pt nanoparticle bioconjugates with (__) and without (---) Cyt c_6.

Table **2-1**: The rates of hydrogen production by Photosystem I/molecular wire/nanoparticle bioconjugates as analyzed by gas chromatography.

Sample	Rate of H_2 Production (μmol H_2 mg Chl^{-1} h^{-1})	Rate of H_2 Production (mol H_2 mol PS I^{-1} s^{-1})
Au nanoparticle, rebuilt PS I, 1,6-hexanedithiol	3.4	0.08
Pt nanoparticle, rebuilt PS I, 1,6-hexanedithiol	9.6	0.23
Pt nanoparticle, rebuilt PS I, 1,6-hexane dithiol, Cyt c_6	49.3	1.17

I/molecular wire/Pt nanoparticle bioconjugates generated 9.6 μmol H_2 mg Chl^{-1} h^{-1}. Addition of 5 μM Cyt c_6 increased the rate of H_2 production by the Pt nanoparticles to 49.3 μmol H_2 mg Chl^{-1} h^{-1}, which indicates that the H_2 evolution is not limited by electron transfer through the molecular wire, but rather by the donor-side reduction of $P700^+$. Appropriate controls were carried out to verify that all components were required for H_2 evolution (Table 2-2).

Table **2-2**: H_2 production rates for control samples. All samples contained 100 mM Na ascorbate and 10 μM DCPIP.

Sample	Rate of H_2 Production (μmol H_2 mg Chl^{-1} h^{-1})
Pt Nanoparticle (Pt NP)	0
Au Nanoparticle (Au NP)	0
Wild Type Photosystem I (WT PS I)	0
Pt NP, WT PS I	0
Au NP, WT PS I	0
Pt NP, WT PS I, 1,6-hexanedithiol	0
Au NP, WT PS I, 1,6-hexanedithiol	0
Pt NP, P700/F_X cores, C13G/C33S variant PsaC, 1,6-hexanedithiol	0
Au NP, P700/F_X cores, C13G/C33S variant PsaC, 1,6-hexanedithiol	0
Pt NP, Rebuilt PS I	0
Au NP, Rebuilt PS I	0
Pt NP, Rebuilt PS I, 1,6-hexanedithiol, no illumintion	0
Au NP, Rebuilt PS I, 1,6-hexanedithiol, no illumintion	0
Pt NP, Cyt c_6	0

No H_2 production was observed for any of the controls that lacked one or more of the components or when wild-type PS I was used in lieu of the rebuilt PS I. These results indicate that light produces the charge-separated state necessary for H_2 evolution. It also demonstrates that the electron can be transferred to the nanoparticle surface only when the reconstituted PS I is covalently attached to the particle surface by 1,6-hexanedithiol. The bifunctional dithiol molecular wire both rescues the iron-sulfur cluster, F_B, and links the protein to the Au or Pt nanoparticle surface, thereby poising PS I at a distance capable of electron transfer at rates faster than the charge recombination time between $P700^+$ and F_B^-.

Photosystem I has previously been utilized in studies that explore its viability in the photocatalytic production of H_2. Low rates of H_2 evolution have been achieved by the platinization of spinach chloroplasts and PS I.[26-29] In those studies, the rate of H_2 evolution was on the order of 0.2 μmol H_2 mg Chl^{-1} h^{-1}, although a rate of 2.0 μmol H_2 mg Chl^{-1} h^{-1} was achieved in one instance.[27-29] Those studies do not address the method by which the Pt is connected to PS I. Direct covalent attachment of PS I to the Pt via the F_B cluster was not possible in those experiments. In addition, a recent study has appeared in which a PS I-H_2ase construct was engineered by fusing the gene encoding the [NiFe]-H_2ase from *Ralstonia eutropha* H16 with the *psaE* gene (which encodes PsaE, a stromal protein of PS I). Subsequent rebinding of the H_2ase-PsaE fusion product onto a PsaE deletion mutant of PS I produced only 0.2 μmol H_2 mg mg Chl^{-1} h^{-1}.[30] Clearly, the ~100-fold difference in H_2 production rates between our PS I/molecular wire/nanoparticle bioconjugates and these of previous studies demonstrates that these alternative approaches are suboptimal for the construction of a H_2-producing PS I adduct. Hence, we conclude that we have developed an improved approach by introducing covalent bonds that direct reducing electrons from the electron transfer cofactor, F_B, to the catalytic nanoparticle surface, which enables the observed high rates of H_2 evolution.

The strategy for the attachment of PS I to a nanoparticle surface via a covalent linkage between an electron transfer cofactor and a molecular wire presented in this communication represents an innovative approach for the binding of proteins to surfaces or other proteins. We therefore consider it feasible to use this approach to link PS I to other external catalysts capable of rapid H_2 generation, such as [FeFe]-H_2ase, [NiFe]-H_2ase, or N_2 reduction.

References

1. Lee, D. W.; Nam, S. E.; Sea, B.; Ihm, S. K.; Lee, K. I. *Catal. Today* **2006**, *118*, 198–204.
2. Croy, J. R.; Mostafa, S.; Lui, J.; Sohn, Y. H.; Cuenya, B. R.; Haruta, M. *Gold Bull.* **2004**, *37*, 27–30.
3. Mizukoshi, Y.; Makise, Y.; Shuto, T.; Hu, J.; Tominaga, A.; Shironita, S.; Tanabe, S. *Ultrasonics Sonochem.* **2007**, *14*, 387–392.
4. Bamwenda, G. R.; Tsubota, S.; Nakamura, T.; Haruta, M. *J. Photochem. Photobiol.* **1995**, *89*, 177–189.
5. Bocuzzi, F.; Chiorino, A.; Manzoli, M.*J. Power Sources* **2003**, *118*, 304–310.
6. Bowker, M.; Mullard, L.; Greaves, J.; James, D.; Soares, J. *Gold Bull.* **2004**, *37*, 170–173.
7. Tang, H.; Berger, H.; Schmid, P. E.; Levy, F. *Solid State Commun*. **1994**, *92*, 267–271.
8. Gibbs, M.; Holaender, A.; Kok, B.; Krampitz, L. O.; San Pietro, A. A report on a workshop held September 5-6, 1973, at Bethesda, MD, supported by NSF under RANN Grant GI 40253 to Indiana University.
9. Antokine, M. L.; Maes, E. M.; Czemuszewiez, R. S.; Breitenstein, C.; Bill, E.; Falzone, C. J.; Balasubramanian, R.; Lubner, C.; Bryant, D. A.; Golbeck, J. H. *Biochim. Biophys. Acta* **2007**, *1767*, 712–724.

10. Stayton, P. S.; Olinger, J. M.; Jiang, M.; Bohn, P. W.; Silgar, S. G. *J. Am. Chem. Soc.* **1992**, *114*, 9298–9299.

11. Huang, C. C.; Huang, Y. F.; Cao, Z.; Tan, W.; Chang, H. T. *Anal. Chem.* **2005**, *77*, 5735–5741.

12. Brast, M.; Bethell, D.; Schiffrin, D. L.; Kiely, C. J. *Ad*V. *Mater.* **1995**, *9*, 795–797.

13. Li, Z.; Chang, S. C.; Williams, R. S. *Langmuir* **2003**, *19*, 6744–6749.

14. Williams, J. A.; Gorman, C. B. *Langmuir* **2007**, *23*, 3103–3105.

15. Frens, G. *Nature – Phys. Sci.* **1973**, *241*, 20-22.

16. Chen, S.; Kimura, K. *J. Phys. Chem. B* **2001**, *105*, 5397-5403.

17. Shen, G.; Zhao, J.; Reimer, S. K.; Antokine, M. L.; Cai, Q.; Weiland, S. M.; Golbeck, J. H.; Bryant, D. A. *J. Biol. Chem.* **2002**, *277*, 20343-20354.

18. Zhao, J.; Warren, P. V.; Li, N.; Bryant, D. A.; Golbeck, J. H. *FEBS Lett.* **1990**, *276***,** 175-180.

19. Antokine, M. L.; Bentrop, D.; Bertini, I.; Luchinat, C.; Shen, G.; Bryant, D. A.; Stehlik, D.; Golbeck, J. H. *J. Biol. Inorg. Chem.* **2000**, *5*, 381-392.

20. Diaz, A.; Navarro, F.; Hervas, M.; Navarro, J. A.; Chavez, S.; Florencio, F. J.; De la Rosa, M. A. *FEBS Lett.* **1994**, *347*, 173-177.

21. Golbeck, J. H.; Parrett, K. G.; Mehari, T.; Jones, K. L.; Brand, J. J. *FEBS Lett.* **1988**, *228*, 268-272.

22. Parrett, K. G.; Mehari, T.; Warren, P. G.; Golbeck, J. H. *Biochim, Biophys. Acta* – **1989**, *973*, 324-332.

23. Lovenberg, W.; Buchanan, B. B.; Babinowitz, J. C.; *J. Biol. Chem.* **1963**, *263*, 3899-3913.

24. Kennedy, M. C.; Kent, T. A.; Emptage, M.; Merkle, H.l Berhert, H.; Munk, E. *J. Biol. Chem.* **1984**, *259*, 14463-14471.

25. Golbeck, J. H.; Lien, S.; San Pietro, A. *Biochem. Biophys. Res. Commun.* **1976**, *71*, 452-458.

26. Evans, B. R.; O'Neill, H. M.; Hutchens, S. A.; Bruce, B. D.; Greenbaum, E. *Nano Lett* **2004**, *4*, 1815–1819.

27. Millsaps, J. F.; Bruce, B. D.; Lee, J. W.; Greenbaum, E. *Photochem. Photobiol.* **2001**, *73*, 630–635.

28. Greenbaum, E. *Science* **1985**, *230*, 1373–1375.

29. Lee, J. W.; Tevault, C. V.; Blankinship, S. L.; Collins, R. T.; Greenbaum, E. *Energy & Fuels* **1994**, *8*, 770–773.

30. Ihara, M.; Nishihara, H.; Yoon, K. S.; Lenz, O.; Friedrich, B.; Nakamoto, H.; Kojima, K.; Honma, D.; Kamachi, T.; Okura, I. *Photochem. Photobiol.* **2006**, *82*, 676–682.

Chapter 3

Maximizing H_2 Production in Photosystem I/Dithiol Molecular Wire/Platinum Nanoparticle Bioconjugates*

Introduction

The direct conversion of sunlight into portable chemical fuels is a promising method to an energy future that does not rely on the combustion of fossil fuels. A viable alternative energy source may be found in hydrogen that can be produced by the conversion of solar energy. Work by our laboratory has focused on the ability of cyanobacterial PS I to photocatalytically generate H_2 when covalently linked to a Au or Pt nanoparticle via a dithiol molecular wire.[1] The molecular wire is attached to PS I by functioning as a thiol-containing rescue ligand to the F_B cluster in a Cys→Gly variant of PsaC. The other end of the molecular wire is attached to the nanoparticle via its second thiol group. When 1,6-hexanedithiol was used as the molecular wire and Pt as the nanoparticle, H_2 was generated at a rate of 49.3 μmol mg Chl^{-1} h^{-1} under continuous illumination. The work presented here seeks to elucidate the factors that govern the rate of H_2 production so as to produce maximal rates in hybrid PS I/molecular wire/Pt nanoparticle bioconjugates.

---

* Grimme, R.A., Lubner, C.E. and Golbeck, J.H., "Maximizing H2 Production in Photosystem I/Dithiol Molecular Wire/Platinum Nanoparticle Bioconjugates" *Dalton Trans.*, **2009**, 10106-10113. - Reproduced by permission of the Royal Society of Chemistry (RSC).

Materials and Methods

Materials

All chemicals were of reagent grade and were used as purchased, without further purification or modification. All solutions were prepared using 18.1 MΩ distilled water or reagent grade solvents.

Platinum Nanoparticle Synthesis

Mercaptosuccinic acid (MSA) stabilized platinum nanoparticles were prepared by the reduction of $H_2[PtCl_6]$.[2] $NaBH_4$ was added to solutions of vigorously stirring $H_2[PtCl_6]$ and MSA at a ratio of 10:1:0.7 for $NaBH_4$/Pt/MSA. Pt nanoparticles with dimensions of 2.89 ± 0.41 nm resulted from this synthesis as determined by TEM analysis of 209 particles (data not shown).

Protein Purification

All proteins were isolated either from the native organism or by expression in *Esherichia coli* BL21 (DE3) cells. Following purification, the proteins were stored at -80 °C until use, unless otherwise stated.

Purification of Photosystem I Complexes from Synechcoccus *sp. PCC 7002*

PS I complexes were purified from *Synechococcus* sp. PCC 7002 thylakoids using

established methods.[3] PS I complexes were isolated by detergent treatment of fragmented thylakoid membranes using 1% Triton X-100 and purified by sucrose density ultracentrifugation. The PS I complexes were resuspended in buffer containing 0.1% Triton X-100 and 15% glycerol in 50 mM Tris buffer, pH 8.3.

Purification of Photosystem I Complexes from Commercially Available Baby Spinach

PS I was purified from baby spinach leaves by following a standard literature protocol with slight modification.[4] Thylakoid membrane fragments were isolated and solubilized in 200 mM KCl and 1% Triton X-100 in 50 mM Tris, pH 8.3. PS I was isolated by sucrose density ultracentrifugation (5-20% sucrose gradients in 50 mM Tris (pH 8.3)) from the solubilized thylakoid fragments. The PS I complexes were resuspended in 50 mM Tris, pH 8.3, buffer containing 0.1% Triton X-100, 15% glycerol, and 200 mM KCl.

Purification of Plastocyanin from Baby Spinach Leaves

Plastocyanin was isolated from 10 kg of commercially available baby spinach leaves following a procedure similar to that previously published.[5, 6] Spinach chloroplasts were isolated by centrifugation at 10000 x g for 10 minutes following homogenization in a 1.25 L blender (Biospec Products) in 50 mM Tris, pH 7.8, containing 0.4 M sucrose. Soluble proteins were precipitated by treatment with ice cold acetone followed by centrifugation at 10000 x g. The pellet was resuspended in 50 mM Tris, pH 7.8 and dialyzed overnight against 2 L of 50 mM Tris, pH 7.8, using 8000 molecular weight cut-off tubing. The dialyzed extract was loaded onto a 3 x 15 cm DEAE Sepharose column that was pre-equilibrated with 50 mM Tris, pH 8.3. The column was washed with several volumes of 50 mM Tris, pH 7.8, and was

eluted with 50 mM Tris, pH 7.8, containing 0.2 M NaCl. Fractions containing plastocyanin were pooled and concentrated over a 3-kDa cutoff membrane. The concentration of the protein was determined using an extinction coefficient of 4900 M^{-1} from the A_{597ox} minus A_{597red} difference spectrum.[6]

Purification of Recombinantly Expressed Cytochrome c_6

Escherichia coli BL21 (DE3) cells were co-transformed with a pBluescript SK+ plasmid containing the *petJ* gene, which encodes the cytochrome c_6 protein from *Synechocystis* sp. PCC 6803, and a pEC86 plasmid, which contains the cytochrome c maturation genes from *Synechocystis* sp. PCC 6803.[7] The proteins were overproduced and cytochrome c_6 was isolated from the periplasmic fraction of the *E. coli* cells following an established protocol.[8] The purified cytochrome c_6 was concentrated over a 3 kDa cutoff membrane. Protein concentration was determined using the extinction coefficient 23000 M^{-1} cm^{-1} at 553 nm from the spectrum of ascorbate-reduced cytochorme c_6.[9]

Purification of Recombinantly Expressed C13G/C33S Variant PsaC

The C13G/C33S variant of the PS I stromal protein PsaC from *Synechococcus* sp. PCC 7002 was overproduced in *E. coli* BL 21 (DE3) cells and purified according to an established protocol.[10] The PsaC variant was reconstituted with iron-sulfur clusters under anaerobic conditions using a previously described procedure.[11] After reconstitution, the presence of the F_A and F_B clusters was verified by low temperature EPR spectroscopy and by iron and acid-labile sulfide analysis.[12, 13] The reconstituted C13G/C33S variant of PsaC was handled anaerobically and stored under liquid N_2 until use.

Purification of Recombinantly Expressed PsaD

The PS I stromal protein, PsaD, from *Synechocystis* sp. PCC 6803 was overproduced in *E. coli* BL21 (DE3) cells and purified following an already established method.[14] Purified protein was concentrated over a 3 kDa cutoff membrane. Protein concentration was determined using standard Bradford assay techniques.[15]

Purification of Recombinantly Expressed Flavodoxin

Flavodoxin from *Synechococcus* sp. PCC 7002 was overproduced in *E. coli* BL21 (DE3) cells and was purified following an established protocol.[16] Purified protein was concentrated over a 3 kDa membrane. Protein concentration was determined using the extinction coefficient for oxidized flavodoxin of 9500 M^{-1} cm^{-1} at 467 nm.[16]

Preparation of P700/F_X Cores

Purified spinach PS I complexes were subjected to 6 M urea to remove the native stromal proteins PsaC, PsaD, and PsaE following a previously established procedure.[17, 18] The removal of the stromal proteins was monitored by observing a decrease in the amplitude of the kinetic phase that corresponds to the charge recombination of $P700^+$ and F_B^- using flash-induced optical spectroscopy at 820 nm (data not shown). The resulting P700/F_X cores were washed extensively, concentrated over a 100 kDa membrane to remove the unbound stromal proteins, and passed over three Quick Spin protein desalting/buffer exchange columns (Roche) loaded with G-25 resin and pre-equilibrated with buffer containing 200 mM KCl and 0.1% Triton X-100 in 50 mM Tris, pH 8.3, to further remove urea.

Rebuilding of Photosystem I from P700/F_X Cores and Recombinant PsaC and PsaD

PS I was reassembled from P700/F_X cores and recombinantly expressed C13G/C33S PsaC and PsaD at a ratio of 1:50:500, under anaerobic conditions.[14] The rebuilt PS I was washed over a 100 kDa membrane to remove any unbound PsaC and PsaD. The rebinding of PsaC and PsaD was confirmed by the reappearance of the ~65 ms kinetic phase that corresponds to the charge recombination between $P700^+$ and F_B^- using flash-induced optical spectroscopy at 820 nm (data not shown).

Plastocyanin Cross-linking to Rebuilt Photosystem I

Plastocyanin was cross-linked to rebuilt PS I following a procedure similar to that previously described.[19] Rebuilt PS I was first buffer-exchanged into 50 mM MES buffer, pH 6.4, containing 5 mM $MgCl_2$ and 0.1% Triton X-100 using a Quick Spin protein desalting/buffer exchange column (Roche) loaded with G-25 resin and pre-equilibrated with the same buffer. Plastocyanin was subjected to buffer exchange into 50 mM PBS buffer, pH 7.4, by passage over a Quick Spin protein column packed with G-25 resin and pre-equilibrated with the same buffer. Rebuilt PS I at 0.2 mg Chl mL^{-1} was first reacted with 5.0 mM *N*-hydroxysulfosuccinimide and 5.0 mM 1-ethyl-3-[3-dimethlyaminopropyl]carbodiimide in 50 mM MES buffer, pH 6.4. The pH was then adjusted to 7.4 using concentrated PBS buffer and $MgCl_2$ was added to a final concentration of 5 mM. Plastocyanin was added (150 μM final concentration) and the cross-linking reaction was allowed to proceed for 2 h at room temperature in the dark after which it was quenched with 100 mM ammonium acetate. The cross-linked proteins were dialyzed twice for 2 hours against 1 L of 50 mM PBS buffer, pH 7.4, using a 30 kDa cut-off dialysis membrane. The

cross-linked proteins were concentrated over a 100 kDa ultrafiltration membrane.

Chlorophyll to P700 Ratio

The ratio of chlorophyll to P700 was determined in samples of *Synechococcus* sp. PCC 7002 PS I, spinach PS I, and rebuilt spinach PS I. The concentration of P700 was determined at 700 nm from the chemically oxidized minus reduced difference spectrum using a method similar to that described in Sonoike and Katoh.[20] Samples contained 30 μg Chl mL^{-1}, 10 mM NaCl, 10 mM $MgCl_2$, and 0.1% Triton X-100 in 50 mM Tris buffer, pH 7.4.[20, 21] The samples were reduced by the addition of a small amount of solid sodium ascorbate or oxidized by the addition of a small grain of solid potassium ferricyanide. The concentration of P700 was determined using the differential extinction coefficient of 64 mM^{-1} cm^{-1} at 700 nm.[22] Difference spectra were recorded on an Olis Cary-14 double-beam spectrophotometer as the average of 10 individual scans. The difference spectrum of 10 averaged scans of non-oxidized minus non-reduced PS I served as the baseline. The chlorophyll concentration of each sample was determined by methanol extraction of cyanobacterial PS I (extinction coefficient A_{663} = 82 mL mg^{-1} cm^{-1}) and acetone extraction of spinach PS I samples using the equation $[Chl_{TOTAL}] = (A_{663} \times 0.0808)+(A_{645} \times 0.202)$ to account for both Chl *a* and Chl *b* in the spinach PS I samples.[23-25] Ratios shown are the average of 3 independent samples.

Measurement of Steady-state Rates of Flavodoxin Reduction

The rate of light-induced reduction of recombinantly expressed flavodoxin by *Synechococcus* sp. PCC 7002, spinach, and rebuilt spinach PS I were assessed as previously described.[26, 27] Samples of 400 μL total volume contained 30 mM flavodoxin, PS I at 30 μg

Chl mL^{-1}, 10 μM DCPIP, 10 mM Na ascorbate, 10 mM NaCl, 10 mM $MgCl_2$, and either plastocyanin (in samples containing spinach or rebuilt spinach PS I) or cytochrome c_6 (in samples containing *Synechococcus* sp. PCC 7002 PS I) at 5 μM in 50 mM Tris buffer, pH 8.3. Actinic light was provided by two Hansatech Ltd. LED arrays, each of which contained 7 high-intensity LEDs (λ_{max} = 670 nm) that were varied from 1 to 100% of the total irradiance, and the absorbance was monitored at 580 nm using a Varian Cary 65 spectrophotometer. The detector was protected from stray light from the actinic light using a shortpass interference filter with bandpass from 400 to 580 nm (Edmund Optics). Rates shown are the average of 3 independent samples.

Assembly of the Photosystem I/Molecular Wire/Pt Nanoparticle Bioconjugates

Photosystem I/molecular wire/Pt nanoparticle bioconjugates were assembled as previously described.[1] Briefly, rebuilt PS I or plastocyanin cross-linked rebuilt PS I (final concentration ≈ 5.0 μg Chl mL^{-1}) was combined in the dark with Pt nanoparticles at a 1:1 molar ratio, and a dithiol molecular wire was added to a final concentration of 200 nM. The dithiol molecular wires were diluted in 95% ethanol unless otherwise specified. Bioconjugates were allowed to assemble for at least 2 h in the dark at room temperature with slight agitation. The bioconjugates were studied within 24 h of assembly.

Steady State Production of H_2

PS I/molecular wire/Pt nanoparticle bioconjugates were evaluated for light-induced H_2 generation. A typical reaction solution at 1.0 mL total volume contained PS I/molecular wire/Pt nanoparticle bioconjugates at 5 μg Chl mL^{-1}, 100 mM Na ascorbate, and 10 μM

DCPIP.[1] Unless otherwise specified, samples were buffered in 50 mM Tris, pH 8.3, containing 10 mM $MgCl_2$ and 10 mM NaCl. Plastocyanin was added to a final concentration of 5 μM in samples in which it was not cross-linked to PS I. No additional plastocyanin was added to samples in which it had previously been cross-linked to PS I.

For all studies, samples were added to sealed, N_2-purged glass vials. The PS I/molecular wire/Pt nanoparticle bioconjugates were illuminated continuously for 6 to 24 h using a Xe arc lamp at a maximum irradiance of 70 μE m^{-2} s^{-1} unless otherwise specified. The beam of white light was filtered through a clear polycarbonate culture flask filled with doubly distilled water to remove both the IR and UV portions of the spectrum. The reaction vial remained at room temperature (20 to 23 °C) for the duration of the illumination.

The amount of H_2 produced by the samples was evaluated by gas chromatography after removing a 200 μL sample of gas from the headspace using a gas-tight, locking syringe. Analysis was performed with a Shimadzu GC-8A gas chromatograph equipped with a thermal conductivity detector (100 mA detector current). Ultra-pure N_2 served as the carrier gas (flow rate = 0.75 mL min^{-1}) to transport the sample through a packed ShinCarbon 80/100 column (2 m x 2 mm).

Plastocyanin Cross-linking Studies

The rate of H_2 production by rebuilt PS I/molecular wire/Pt nanoparticle bioconjugates was investigated in samples that contained both free (non-cross-linked) and cross-linked plastocyanin to determine whether diffusion of the electron donor to P700 had an influence on the rate of H_2 generation.

Ionic Concentration Studies

$MgCl_2$ and NaCl were added at various concentrations to plastocyanin cross-linked rebuilt PS I/1,6-hexanedithiol/Pt nanoparticle bioconjugate samples. The concentration of NaCl was varied from 0 to 50 mM in a background of 10 mM $MgCl_2$ while the concentration of $MgCl_2$ was varied from 0 to 50 mM in a constant background of 10 mM NaCl .

pH Studies

Samples were prepared using the plastocyanin cross-linked rebuilt PS I/1,6-hexanedithiol/Pt nanoparticle bioconjugates but poised at pH values from 6.0 to 10.0 using appropriate buffers. The identity of the buffer had no effect on the rate of light-induced H_2 generation. The samples studied from pH 7.0 to pH 9.0 were in 50 mM Tris (at pH 7.0, 8.0, and 9.0). The sample studied at pH 6.0 was buffered in 50 mM MES, and the sample studied at pH 10.0 was in 50 mM CAPS.

Molecular Wire Studies

1,3-propanedithiol, 1,6-hexanedithiol, 1,8-octanedithiol, 1,10-decanedithiol, and 1,4-benzenedithiol were diluted in 95% ethanol and 4,4'-biphenyldithiol was diluted in a 50% (v/v) solution of dimethylformamide/ethanol to a final concentration of 10 μM. The PS I bioconjugates were assembled at 200 nM final concentration of the molecular wire.

Light Saturation Studies

The light intensity was varied from 0.6% to 100% of the initial intensity with the use of

neutral density optical filters. The rate of light-induced H_2 production was evaluated at 5 different light intensities.

Results and Discussion

Chlorophyll to P700 Ratio

The ratio of Chl to P700 was determined in *Synechococcus* sp. PCC 7002 PS I, native spinach PS I, and rebuilt spinach PS I (Table 3-1). The ratio of Chl to P700 in *Synechococcus* sp PCC 7002 was 92:1, the ratio in native spinach PS I was 155:1, and the ratio in rebuilt spinach PS I was 143:1. The latter two values indicate that there was little or no damage in the process of preparing the F_X cores or in rebuilding the spinach PS I complexes. The spinach and cyanobacterial ratios of Chl to P700 agree well with previously published values.[28-30] The ratios are employed here in the determination of rates of flavodoxin reduction and of H_2 production, which are expressed on a per PS I basis, (as there is one P700 per PS I reaction center).

Table **3-1**: The ratio of Chl:P700 in various PS I samples.

PS I Sample	Chl:P700 Ratio
Synechococcus sp. PCC 7002	91.5 ± 7.0
Native Spinach	155.2 ± 15.4
Rebuilt Spinach	143.7 ± 13.9

Table **3-2**: The rate of flavodoxin reduction by various PS I samples as a function of the total chlorophyll concentration and as a function of PS I concentration extrapolated to saturating light intensities.

PS I Sample	Rate of Fld reduction (μmol Fld mg Chl^{-1} h^{-1})	Rate of Fld reduction (mol Fld mol PS I^{-1} s^{-1})
Synechococcus sp. PCC 7002	1053	24.6
Native Spinach	2208	85.2
Rebuilt Spinach	1862	66.5

Photosystem I Electron Throughput Studies

The rate of flavodoxin reduction by *Synechococcus* sp. PCC 7002 PS I and spinach PS I is a good indicator of the overall electron throughput. The rates of flavodoxin reduction for spinach PS I (both native and rebuilt) are higher than the rates of flavodoxin reduction by *Synechococcus* sp. PCC 7002 PS I, especially at low light intensities. Rates were converted to a per PS I reaction center basis due to the fact that spinach PS I has a higher ratio of Chl to P700 (Table 3-2). When the rates are extrapolated to saturating light intensity using Michealis-Menten kinetics, maximum rates for flavodoxin reduction were still found to be higher for spinach PS I on a reaction center basis than for *Synechococcus* sp. PCC 7002 PS I (Table 3-2).

Due to the higher electron throughput of spinach PS I under both saturating and non-

saturating light conditions, it was used in subsequent experiments that aim at maximizing the rate of light-induced H_2 generation in the PS I/molecular wire/nanoparticle bioconjugates. Spinach PS I comprises 16 subunits, which support 19 additional chlorophyll molecules, thereby serving to supplement the antenna.[31, 32] Additional chlorophyll molecules are also bound to the LHC-1 proteins, each of which consist of four trans-membrane α-helices. [33, 34] These additional chlorophyll molecules result in a higher ratio of Chl to P700 and serve to increase the optical cross-section of PS I. Provided there are no additional rate limitations on the donor or acceptor sides, this should translate to a higher rate of H_2 production per PS I complex at nonsaturating light intensities. There is an extension in a luminal loop of PsaF that is not present in cyanobacterial PS I.[35, 36] This extension increases the strength and specificity of the interaction between spinach PS I and plastocyanin, which may provide a more favorable interaction than that between cyanobacterial PS I and cytochrome c_6, and has been implicated in a higher cross-linking efficiency.[37-39] PS I from spinach is a monomer (*i.e.* a single PsaA/B heterodimer and the associated proteins that make up a single reaction center) whereas cyanobacterial PS I is a trimer.[33, 40, 41] A possible decrease in steric hindrance due to the use of spinach PS I monomers may also aid in a more efficient PS I/nanoparticle linkage by the dithiol molecular wire.

Elimination of Diffusional Limitations

As was shown by Greenbaum and coworkers, donor-side diffusional limitations play a role in determining the overall rate of H_2 production in platinized PS I.[19] By cross-linking the protein that donates electrons to $P700^+$, the overall production of H_2 was shown to increase.[19]

The cross-linking of plastocyanin to spinach PS I with the zero-length cross-linker

EDC eliminates diffusional rate limitations in the PS I/molecular wire/Pt nanoparticle bioconjugates. Rates of H_2 production for PS I/1,6-hexanedithiol/Pt nanoparticle bioconjugates were evaluated with plastocyanin both free in solution and when chemically cross-linked to PS I.

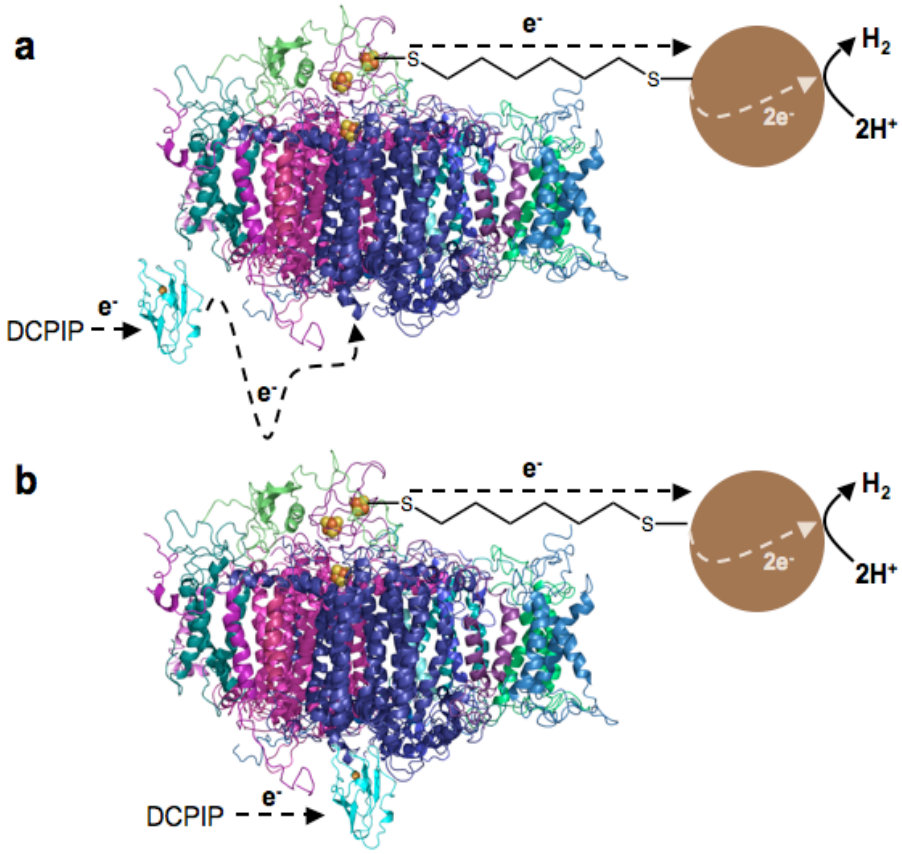

Figure **3-1**: When plastocyanin is free in solution (a) the rate of H_2 production is 52.7 µmol H_2 mg Chl^{-1} h^{-1} and is limited by the diffusion of the electron donating protein. Chemical cross-linking of plastocyanin to rebuilt Photosystem I (b) increases the rate of H_2 production by the PS I/1,6-hexanedithiol/Pt nanoparticle bioconjugates to 100.6 µmol H_2 mg Chl^{-1} h^{-1} which constitutes an approximate 2 fold enhancement.

The rate of H_2 production for the cross-linked plastocyanin bioconjugate was 100.6 μmol H_2 mg Chl^{-1} h^{-1} compared to 52.7 μmol H_2 mg Chl^{-1} h^{-1} for the non-cross-linked sample. The PS I and plastocyanin no longer need to rely on slow diffusion chemistry for electron transfer to occur, (Figure 3-1) thereby accelerating the rate of electron donation to $P700^+$. This leads to an increase in the rate of H_2 production by a factor of two. These results agree with Greenbaum's studies on the cross-linking of plastocyanin to platinized PS I. Plastocyanin cross-linked to spinach PS I was used in the remainder of our studies.

Bioconjugate Solution Studies

The solution pH and ionic strength play a large role in the interaction of electron donors and electron acceptors with the PS I complex.[16, 42] However, these factors should have little or no effect on the donation of electrons from plastocyanin to PS I or from PS I to the Pt nanoparticle in this study due to the fact that both are covalently linked to PS I either through EDC cross-linking or by the dithiol molecular wire. The main influence of the solution characteristics should be on the H^+ adsorption and H_2 catalysis at the nanoparticle surface.

Ionic Concentration Dependence of H_2 Evolution

While the ionic strength of a solution has been shown to have a strong effect on the interactions between PS I and free plastocyanin or cytochrome c_6, it remained to be seen whether the ionic strength modulated the generation of H_2 in bioconjugates in which plastocyanin was cross-linked to PS I. Both $MgCl_2$ and NaCl concentrations were varied independently and the H_2 production was assessed for PS I/molecular wire/Pt nanoparticles maintained at pH 8.3 in Tris buffer.

Light-induced H_2 generation by the PS I/molecular wire/Pt nanoparticle bioconjugates was relatively independent of NaCl concentration (data not shown). The same is true for $MgCl_2$ except that concentrations greater than 25 mM led to irreversible

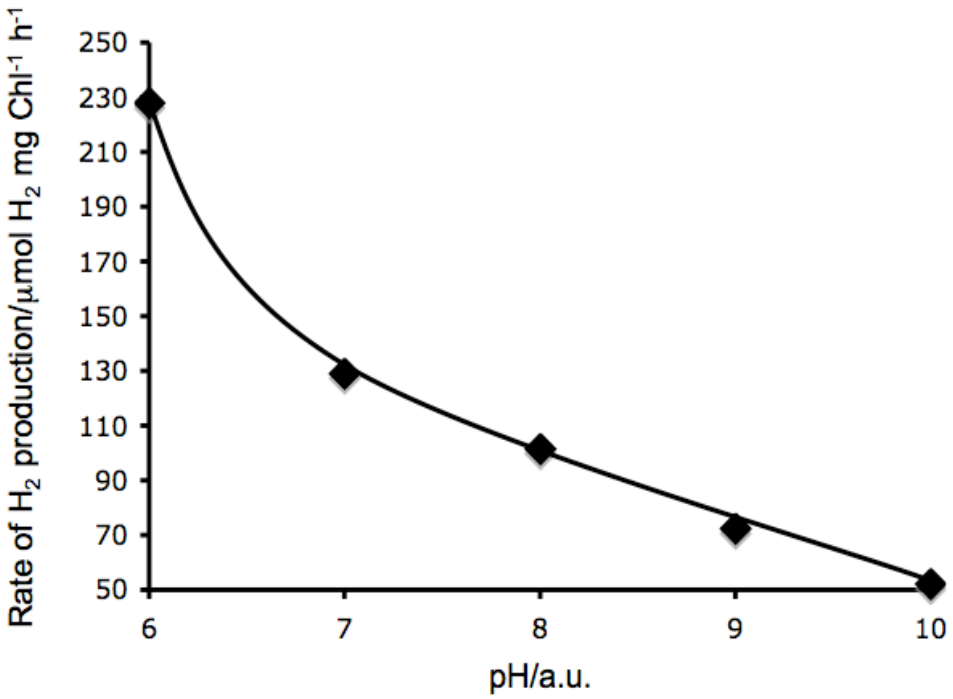

Figure **3-2**: Effect of pH on the rate of light-driven H_2 production by plastocyanin cross-linked PS I/1,6-hexanedithiol/Pt nanoparticle bioconjugates. The bioconjugates are unstable below pH 6.0.

aggregation of the samples. The bioconjugates flocculated, due to a disruption in the coulombic repulsion forces that maintain aqueous nanoparticle preparations in solution.[43]

pH Dependence of H_2 Evolution

In much the same way that semiconductor-supported Au and Pt are able to evolve H_2, the PS I/molecular wire/Pt nanoparticle bioconjugate reduces H^+ ions that are present in water to generate H_2 at the nanoparticle surface.[44] Samples were studied at pH values from pH 6.0 to pH 10.0, which is within the range of stability of the bioconjugates, to determine whether the H^+ concentration has an influence on the rate of H_2 generation.

Bioconjugates at lower pH values generated H_2 at higher rates than samples at higher pH values. The rate of H_2 generation at pH 6.0 was 228.0 μmol H_2 mg Chl^{-1} h^{-1} and at pH 10.0 was 52.3 μmol H_2 mg Chl^{-1} h^{-1} (Figure 3-2). The overall trend in H_2 production as a function of pH appears to be a sharp decrease as the pH increases.

Effect of Molecular Wire Length and Bond Saturation on H_2 Production

To determine the effect of distance between PS I and the Pt nanoparticle and the influence of the aromaticity of the molecular wire on the rate of H_2 production by the PS I/molecular wire/Pt nanoparticle bioconjugate, dithiols of varying length and bond saturation were employed in their construction (Table 3-3).

The fastest rate overall was found using the aromatic wire 1,4-benzenedithiol, and the rate dropped as a second aromatic ring was added. The bioconjugates with the conjugated bonds have higher rates of H_2 generation than do bioconjugates with aliphatic molecular wires of similar length.

For aliphatic dithiols, the rate of H_2 production decreased as the length of the molecular wire increased. A notable exception to this trend was observed in the H_2 production rates for bioconjugates constructed with 1,3-propanedithiol for which the light-

induced H_2 generation rate was considerably lower than expected.

The length of 1,3-propanedithiol may not be sufficient to allow for efficient covalent linkage between PS I and the Pt nanoparticle. Additionally, as the length of the carbon chain decreases, the effectiveness for shielding proteins from denaturation on metal surfaces also decreases.[45, 46] Because the carbon chain in the 1,3-propanedithiol is so short, if the two are

Table **3-3**: Molecular wire length and bond saturation affect the rate of H_2 production by plastocyanin cross-linked rebuilt spinach PS I/dithiol molecular wire/Pt nanoparticle bioconjugates.

Molecular wire	Rate of H_2 production (μmol H_2 mg Chl^{-1} h^{-1})	Rate of H_2 production (mol H_2 mol PS I^{-1} s^{-1})
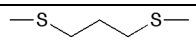 1,3-propanedithiol	2.5	0.09
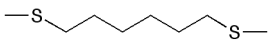 1,6-hexanedithiol	98.6	3.52
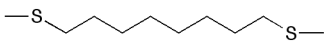 1,8-octanedithiol	49.0	1.75
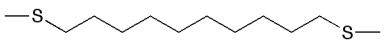 1,10-decanedithiol	16.1	0.57
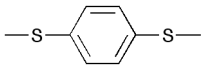 1,4-benzenedithiol	150.5	5.37
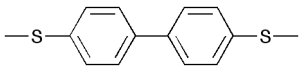 4,4'-biphenyldithiol	92.5	3.31

successfully linked by the molecular wire, some protein denaturation may occur. Depending

on the degree of denaturation, the electron transfer capabilities of PS I may be reduced or lost and H_2 production rates would therefore be lower.

An electron passing through the molecular wire competes with the backreaction of the charge-separated state between $P700^+$ and F_B^-. For quantum efficiencies greater than 50%, an electron must be transferred from F_B through the molecular wire at times faster than 65 ms. As the forward rates become faster, for example due to shorter distances, the quantum efficiency should increase until the rate is so rapid that the competition with the backreaction becomes negligible. The sulfur to sulfur lengths were calculated to be 11.5 Å and 8.2 Å by DFT energy minimzations of 1,6-hexanedithiol and 1,4-benzenedithiol, respectively. It has been shown that for wire lengths between 6.6 Å and 28 Å, electron transfer occurs on the picosecond timescale.[47] While the molecular wires employed in our study are less conjugated or fully saturated, they should allow forward electron transfer times on the order of nanoseconds or possibly sub-nanoseconds. This is roughly three to four orders of magnitude lower than the charge recombination, which means that the back reaction is not significantly competing with electron transfer through the molecular wires. Therefore the variation in H_2 production rates with the wires employed in this study cannot be explained by competition between forward electron transfer through the molecular wire and charge recombination between F_B^- and $P700^+$.

One possibility is that the efficiency of the coupling between PS I and the nanoparticle may vary for the different molecular wires, thereby modulating the rates. H_2 production rates are highly dependent on the proper assembly of the bioconjugate, as they are normalized to chlorophyll concentration. Another possibility is that the construction of these bioconjugates is not 100% efficient with any wire, which may result in two PS I complexes being connected. No hydrogen would be observed if this type of construct were created. Because this portion of non-hydrogen evolving complexes is present in our solutions we are

most likely underestimating the H_2 production rates.

Effect of Light Intensity on H_2 Generation

The generation of H_2 by PS I/molecular wire/Pt nanoparticle bioconjugates is light

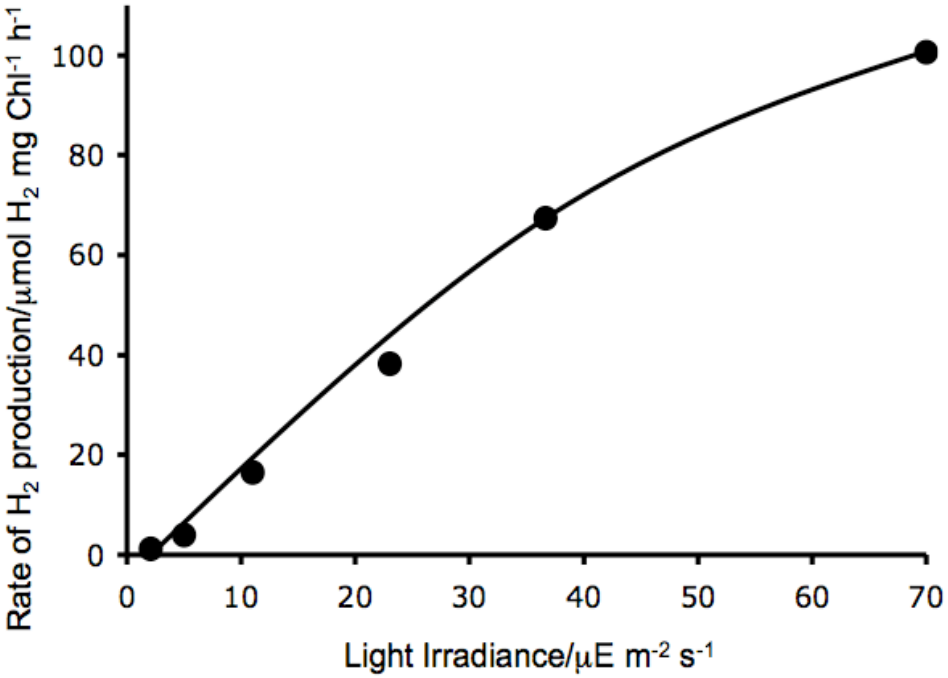

Figure **3-3**: The effect of light intensity on light-driven H_2 production by plastocyanin cross-linked PS I/1,6-hexanedithiol/Pt nanoparticle bioconjugates. The plot follows Michaelis-Menten kinetics (not shown).

dependent. Therefore light can be considered a substrate in the reaction, and the generation of H_2 is expected to follow Michaelis-Menten kinetics. By varying the intensity, the V_{max} can

be obtained, which corresponds to the rate of H_2 generation at saturating light intensities.

The intensity of the illuminating radiation was varied from 5 μE m^{-2} s^{-1} to 70 μE m^{-2} s^{-1} using neutral density filters which uniformly block all wavelengths of light from 350 to 800 nm.

The highest rate of H_2 production was observed at 70 μE m^{-2} s^{-1}, although it is clear from this plot that we were unable to fully saturate the sample given the intensity of our illumination source (Figure 3-3). As expected, the generation of H_2 by the bioconjugates followed Michaelis-Menten kinetics. The maximum rate of H_2 production by the plastocyanin cross-linked PS I/1,6-hexanedithiol/Pt nanoparticle bioconjugates at saturating light intensity was calculated to be 205.6 μmol H_2 mg Chl^{-1} h^{-1} by determining V_{max} from fitting the data to the Michaelis-Menten kinetic equation. This value is twice the observed rate at our maximum available illuminating intensity.

Maximization of H_2 Production Rates

We have shown that a number of factors influence the rates of light-induced H_2 production by the PS I/molecular wire/Pt nanoparticle bioconjugates. By changing each factor iteratively, the conditions that result in the maximum rate of light-driven H_2 generation were obtained. The best rate was found in bioconjugates constructed with plastocyanin cross-linked to PS I and 1,4-benzenedithiol as the molecular wire (Figure 3-4). This sample was illuminated as a thin film at a light intensity of 70 μE m^{-2} s^{-1} in a solution containing 10 mM NaCl, 10 mM $MgCl_2$, and buffered in MES at pH 6.0. A rate of 312 μmol H_2 mg Chl^{-1} h^{-1} (11.2 mol H_2 mol PS I^{-1} s^{-1}) was observed for this bioconjugate sample. This rate reflects an approximate 6 fold increase over the non-cross-linked bioconjugate buffered at pH 8.3, using 1,6-hexanedithiol as the molecular wire. When extrapolated to saturating

light intensities, the maximum rate would increase to 638 μmol H_2 mg Chl^{-1} h^{-1}.

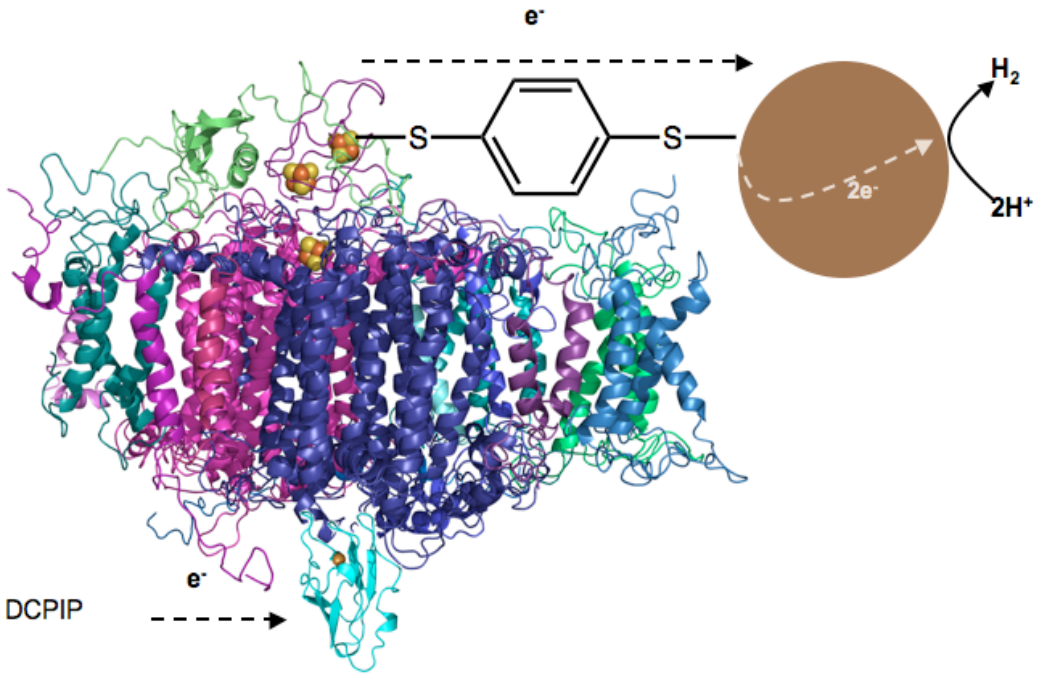

Figure **3-4**: H_2 production rates were maximized by constructing a bioconjugate that consisted of plastocyanin cross-linked PS I, 1,4-benzenedithiol as the molecular wire, and Pt nanoparticles. The system was buffered in MES (pH 6.0) and held at 10 mM NaCl and 10 mM $MgCl_2$. The sample was illuminated as a thin film at the maximum available lamp intensity.

Conclusions

PS I-based hybrid biological systems constitute a viable option for converting solar energy to H_2. The PS I/dithiol molecular wire/Pt nanoparticle bioconjugate system described here is highly tailorable. Iterative changes to the system have been shown to influence the rate of light-driven H_2 evolution by the bioconjugates. The rate of H_2 production by PS I/molecular wire/nanoparticle bioconjugates has been optimized to yield a high rate of light-induced H_2 production. The next step in PS I-based systems is a designed Photosystem I/dithiol molecular wire/[FeFe]-hydrogenase complex that is currently under construction.

References

1. R. A. Grimme, C. E. Lubner, D. A. Bryant and J. H. Golbeck, *J. Am. Chem. Soc.*, 2008, **130**, 6308-6309.
2. S. H. Chen and K. Kimura, *J. Phys. Chem. B*, 2001, **105**, 5397-5403.
3. G. Z. Shen, J. D. Zhao, S. K. Reimer, M. L. Antonkine, Q. Cai, S. M. Weiland, J. H. Golbeck and D. A. Bryant, *J. Biol. Chem.*, 2002, **277**, 20343-20354.
4. J. H. Golbeck, in *Methods in Enzymology*, Academic Press, Inc., Editon edn., 1980, vol. 69, pp. 129-141.
5. W. L. Ellefson, E. A. Ulrich and D. W. Krogman, in *Methods in Enzymology*, Academic Press, Inc., Editon edn., 1980, vol. 69, pp. 223-228.
6. S. Katoh, I. Shiratori and A. Takamiya, *J. Biochem.*, 1962, **51**, 32.
7. A. Diaz, F. Navarro, M. Hervas, J. A. Navarro, S. Chavez, F. J. Florencio and M. A. Delarosa, *FEBS Lett.*, 1994, **347**, 173-177.

8. M. Hervas, F. Navarro, J. A. Navarro, S. Chavez, A. Diaz, F. J. Florencio and M. A. De la Rosa, *FEBS Lett.*, 1993, **319**, 257-260.

9. M. Paumann, M. Feichtinger, M. Bernroitner, J. Goldfuhs, C. Jakopitsch, P. G. Furtmuller, G. Regelsberger, G. A. Peschek and C. Obinger, *FEBS Lett.*, 2004, **576**, 101-106.

10. M. L. Antonkine, D. Bentrop, I. Bertini, C. Luchinat, G. Z. Shen, D. A. Bryant, D. Stehlik and J. H. Golbeck, *J. Biol. Inorg. Chem.*, 2000, **5**, 381-392.

11. W. Lovenberg, J. C. Rabinowitz and B. B. Buchanan, *J. Biol. Chem.*, 1963, **238**, 3899-&.

12. M. C. Kennedy, T. A. Kent, M. Emptage, H. Merkle, H. Beinert and E. Munck, *J. Biol. Chem.*, 1984, **259**, 4463-4471.

13. J. H. Golbeck, S. Lien and A. San Pietro, *Biochem. Bioph. Res. Co.*, 1976, **71**, 452-458.

14. J. D. Zhao, P. V. Warren, N. Li, D. A. Bryant and J. H. Golbeck, *FEBS Lett.*, 1990, **276**, 175-180.

15. M. M. Bradford, *Anal. Biochem.*, 1976, **72**, 248-254.

16. J. D. Zhao, R. G. Li and D. A. Bryant, *Anal. Biochem.*, 1998, **264**, 263-270.

17. J. H. Golbeck, K. G. Parrett, T. Mehari, K. L. Jones and J. J. Brand, *FEBS Lett.*, 1988, **228**, 268-272.

18. K. G. Parrett, T. Mehari, P. G. Warren and J. H. Golbeck, *Biochim. Biophys. Acta*, 1989, **973**, 324-332.

19. B. R. Evans, H. M. O'Neill, S. A. Hutchens, B. D. Bruce and E. Greenbaum, *Nano Lett.*, 2004, **4**, 1815-1819.

20. K. Sonoike and S. Katoh, *Biochim. Biophys. Acta*, 1988, **935**, 61-71.

21. I. Terashima, S. Funayama and K. Sonoike, *Planta*, 1994, **193**, 300-306.

22. T. Hiyama and B. Ke, *Biochim. Biophys. Acta*, 1972, **267**, 160-&.

23. G. Mackinney, *J. Biol. Chem.*, 1941, **140**, 315-322.

24. D. I. Arnon, *Plant Physiol.*, 1949, **24**, 1-15.

25. R. J. Porra and L. H. Grimme, *Anal. Biochem.*, 1974, **57**, 255-267.

26. U. Muhlenhoff, J. D. Zhao and D. A. Bryant, *Eur. J. Biochem.*, 1996, **235**, 324-331.

27. Q. Xu, Y. S. Jung, V. P. Chitnis, J. A. Guikema, J. H. Golbeck and P. R. Chitnis, *J. Biol. Chem.*, 1994, **269**, 21512-21518.

28. Y. R. Zhang, A. Nakamura, Y. Kuroiwa, Y. Kato and T. Watanabe, *FEBS Lett.*, 2008, **582**, 1123-1128.

29. A. Nakamura, T. Suzawa, Y. Kato and T. Watanabe, *FEBS Lett.*, 2005, **579**, 2273-2276.

30. A. Nakamura, M. Akai, E. Yoshida, T. Taki and T. Watanabe, *Eur. J. Biochem.*, 2003, **270**, 2446-2458.

31. T. Morosinotto, M. Ballottari, F. Klimmek, S. Jansson and R. Bassi, *J. Biol. Chem.*, 2005, **280**, 31050-31058.

32. A. Ben-Shem, F. Frolow and N. Nelson, *Photosynth. Res.*, 2004, **81**, 239-250.

33. E. J. Boekema, P. E. Jensen, E. Schlodder, J. F. L. van Breemen, H. van Roon, H. V. Scheller and J. P. Dekker, *Biochemistry*, 2001, **40**, 1029-1036.

34. A. Amunts, O. Drory and N. Nelson, *Nature*, 2007, **447**, 58-63.

35. J. Farah, F. Rappaport, Y. Choquet, P. Joliot and J. D. Rochaix, *EMBO J.*, 1995, **14**, 4976-4984.

36. M. Hippler, F. Drepper, W. Haehnel and J. D. Rochaix, *P. Natl. Acad. Sci. USA*, 1998, **95**, 7339-7344.

37. M. Hervas, J. A. Navarro, A. Diaz, H. Bottin and M. A. De la Rosa, *Biochemistry*, 1995, **34**, 11321-11326.

38. M. Hervas, J. A. Navarro and M. A. De la Rosa, *Accounts Chem. Res.*, 2003, **36**, 798-805.

39. M. Hervas, A. Diaz-Quintana, C. A. Kerfeld, D. W. Krogmann, M. A. De la Rosa and J. A. Navarro, *Photosynth. Res.*, 2005, **83**, 329-333.

40. E. J. Boekema, R. M. Wynn and R. Malkin, *Biochim. Biophys. Acta*, 1990, **1017**, 49-56.

41. A. Kitmitto, A. O. Mustafa, A. Holzenburg and R. C. Ford, *J. Biol. Chem.*, 1998, **273**, 29592-29599.

42. P. Setif, *BBA-Bioenergetics*, 2001, **1507**, 161-179.

43. B. V. Enustun and J. Turkevich, *J. Am. Chem. Soc.*, 1963, **85**, 3317.

44. G. R. Bamwenda, S. Tsubota, T. Nakamura and M. Haruta, *J. Photochem. Photobio. A*, 1995, **89**, 177-189.

45. M. J. Tarlov and E. F. Bowden, *J. Am. Chem. Soc.*, 1991, **113**, 1847-1849.

46. D. D. Schlereth, in *Biosensors and modern biospecific analytical techniques*, ed. L. Gorton, Elsevier, Editon edn., 2005, vol. 44, pp. 1-53.

47. H. D. Sikes, J. F. Smalley, S. P. Dudek, A. R. Cook, M. D. Newton, C. E. D. Chidsey and S. W. Feldberg, *Science*, 2001, **291**, 1519-1523.

Chapter 4

Functionalizing Gold Electrodes with Photosystem I

Introduction

Photosystem I/dithiol molecular wire/nanoparticle bioconjugates are capable of the photocatalytic production of H_2.[1,2] These solution-based systems utilize sacrificial electron donating species and diffusion chemistry to supply electrons to the photocatalytic system. Unfortunately, diffusion of electron donating species is slow, and may be the rate-limiting step to these systems. Additionally, while the use of sacrificial electron donors is convenient for small-scale laboratory investigations, their use can become costly over the lifetime of a device or if manufactured on a large scale. To this end, efforts are underway to directly link the photocatalytic system to a gold electrode that would both eliminate diffusion of electron donating species and the need for sacrificial donors.

Many strategies exist for the functionalization of gold electrodes with PS I. Direct attachment of PS I to the electrode may be possible using a variety of alkanethiol self-assembled monolayers (SAMs) with different ω-functionalities. Additionally, an intervening layer of cytochrome c_6 may be used to aid in the docking of the photocatalytic system to the gold electrode. Each of these strategies will be addressed individually.

Direct Attachment of Photosystem I on Gold Electrodes

The attachment of photosynthetic reaction centers to gold electrodes has been investigated for use in photovoltaic devices and nanoscale molecular electronics as well as for investigating their electrochemical and photoelectrochemical properties.[3-16] Typical methods for the adsorption of PS I onto SAMs on gold electrodes are through physical bond or electrostatic interactions.[3-11] Additionally, PS I and bacterial reaction centers (RCs) has been linked to a gold electrode through the specific amino acid variations or poly-histidine tags created within the protein complexes.[12-16] These attachment strategies result in PS I and RCs either being randomly oriented on the surfaces or oriented specifically with either the lumenal or stromal interfaces proximal to the electrode surface.

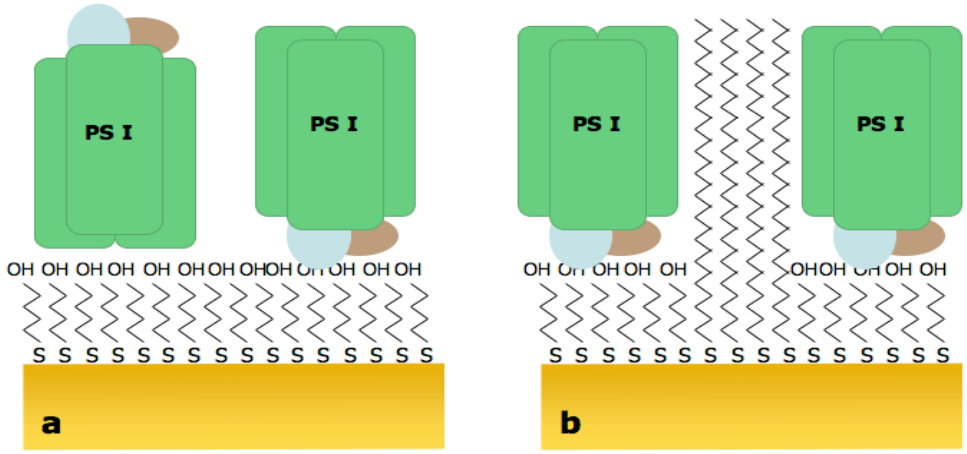

Figure **4-1**: Photosystem I physisorbs onto hydroxyl terminated alkanethiol SAMs (a). Backfilling with longer methyl terminated alkane chains (b) prevents solution phase redox molecules from contacting the electrode surface and dissipating established photocurrents.

Attachment of Wild Type Photosystem I

The adsorption of PS I onto hydroxyl and carboxyl terminated alkanethiol SAMs was determined to be the most favorable in a study that examined the influence of the ω-functionality presented to the protein on the physisorption of PS I.[3] Most studies have focused on the use of hydroxyl terminated SAMs prepared with alkanethiols of varying length.[3-7] The adsorption of PS I onto hydroxyl terminated SAMs results in 30% of the protein complexes in random orientation and 70% oriented with P700 proximal to the electrode.[4] This attachment strategy has been used to examine the electrochemical and photoelectrochemical properties of PS I as well as to determine the electrostatic potentials of single reaction centers.[5,6] Further studies have backfilled areas where no PS I has adsorbed to the hydroxyl terminated SAM with longer alkyl alkanethiols in an effort to prevent solution-phase redox molecules from coming close to the electrode surface and dissipating the photocurrent.[7]

Additionally, PS I can be covalently immobilized on electrode surfaces by specific reaction of exposed lysine residues with the aldahyde group of terephthaldialdahyde (TPDA) to form imine bonds.[8,9] This method of attachment results in either the stromal or lumenal interfaces of PS I proximal to the electrode surface as lysine residues are present on both interfaces. One study performs the functionalization of surfaces under vacuum in order to evaporate solvent and decrease the time involved in PS I adsorption.[8] The use of nanoporous gold leaf electrodes functionalized with TPDA-capped SAMs enables a higher photocurrent measurement due to increased number of PS I complexes bound to the porous substrate in comparison to the flat, two-dimensional subtrates (Figure 4-2-a).[9]

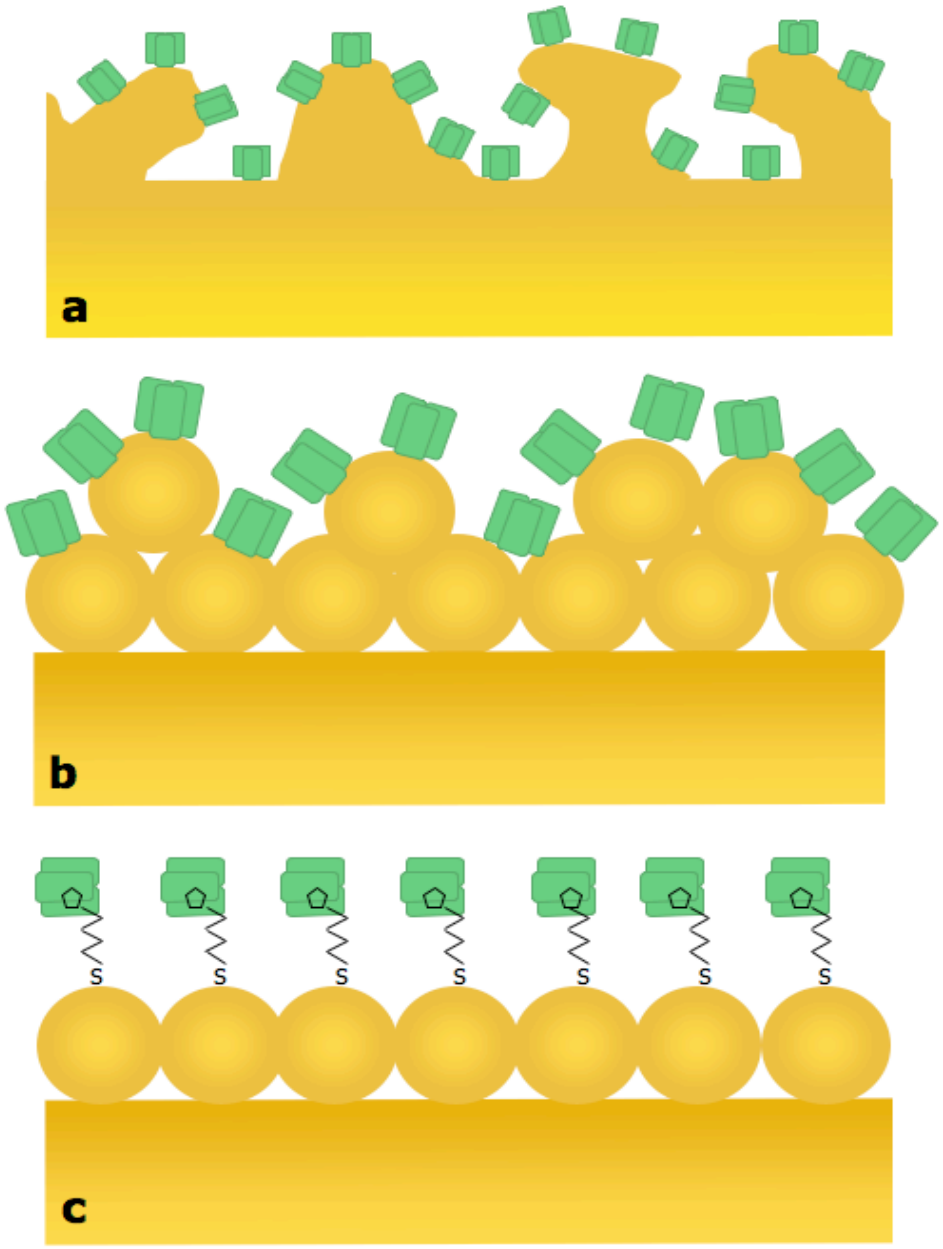

Figure **4-2**: PS I has been attached to three dimensional structured gold substrates by a variety of methods. TPDA was used to covalently bind PS I to the electrode surface of nanoporous gold leaf electrodes (a) through imine bonds. 3-mercapto-1-propanesulfonic acid was utilized to link PS I to Au nanoparticles that were precipitated onto gold electrodes (b). Artificial vitamin K1 on Au nanoparticles was used to reconstitute PS I and the assembly was bound to gold electrodes (c).

The use of three-dimensional substrates was also used in several other studies in which gold nanoparticles are precipitated or covalently bound to gold electrodes.[10,11] PS I was physisorbed onto an electrode that was modified by the precipitation of gold nanoparticles via electrostatic interaction between the stromal interface of the protein complex and a 3-mercapto-1-propanesulfonic acid SAM (Figure 4-2-b).[10] Photocurrent enhancements were observed for this system due to the larger number of PS I protein complexes adsorbed onto the three-dimensional substrates.[10] In another study, PS I that had been extracted with ether to remove the phyloquinone was covalently immobilized onto Au nanoparticles.[11] An artificial vitamin K1 (phyloquinone) was synthesized to contain a sulfhydryl group at the end of the tail portion of the molecule. This artificial vitamin K1 was then used to functionalize the Au nanoparticles. These vitamin K1 capped Au nanoparticles were then used to reconstitute the extracted PS I and this assembly was covalently linked to a gold electrode by 1,4-benzenedimethanethiol. This assembly generated photocurrents and was used in an imaging application (Figure 4-2-c).[11]

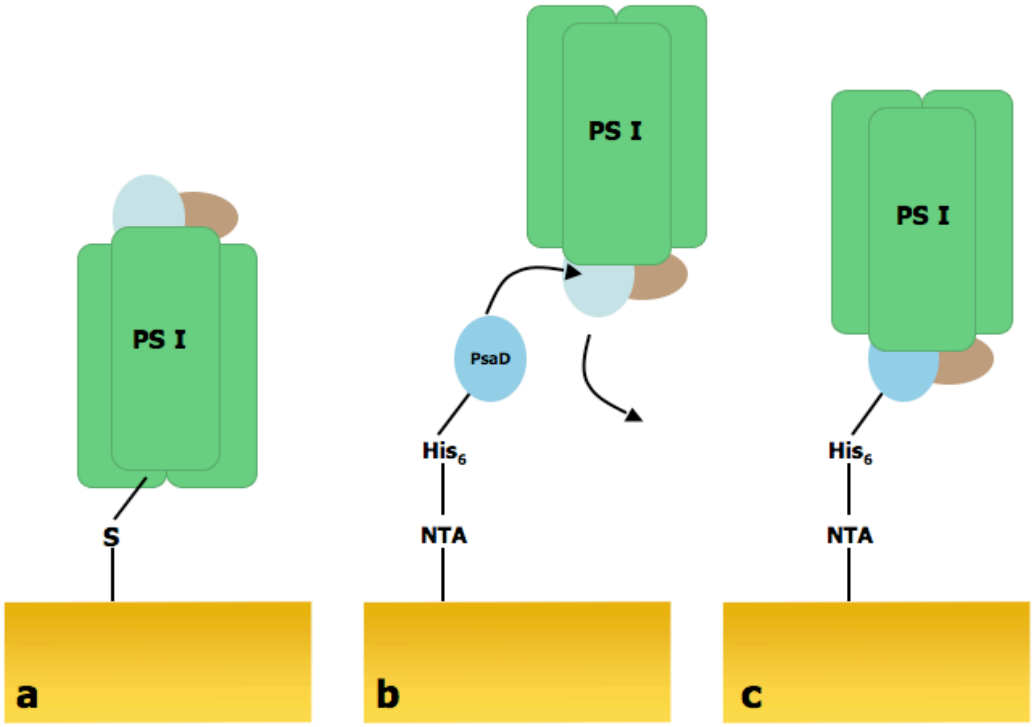

Figure **4-3**: Photosystem I mutants bind to gold electrodes. Cysteine mutants of PS I directly adsorb onto gold electrodes (a). Poly-histidine tagged PsaD binds to Ni-NTA functionalized gold electrodes (b) and displaces intrinsic PsaD to link PS I to the electrode surface (c).

Attachment of Mutant Photosystem I and Bacterial Reaction Centers

While the attachment of PS I on gold electrodes has been successful using the wild type proteins, a variety of mutant PS I and RCs have been covalently linked to gold electrodes. These altered protein complexes include the introduction of surface-located cysteine residues and the insertion of a polyhistidine tag.[12-16]

Cysteine mutants of PS I (D479C, S499C, S599C, and Y634C) were created in the cyanobacterium *Synechocystis* sp. PCC 6803 that introduced cys residues at the lumenal interface PS I.[12] These mutants of PS I were all able to be reacted with biotin-maleimide which confirmed the surface location of the cys residues. All were able to bind to bare gold electrode surfaces and photocurrents were established for each of the mutants (Figure 4-3-a).[12] Additional studies showed that an electrode functionalized with these PS I cysteine mutants was capable of establishing a photocurrent even after drying the protein layer.[13]

Ni-NTA capped gold electrode surfaces have been used for the immobilization of a variety of proteins, including PS I and RCs.[14-16] A single His_6 tag was introduced to PS I by engineering the PsaD subunit.[14] This C-terminally tagged PsaD protein was recombinantly expressed in *E. coli* BL21 (DE3) cells and was immobilized onto a Ni-NTA gold electrode surface (Figure 4-3-b). Native PS I was introduced and the intrinsic PsaD was allowed to exchange with the surface-immobilized PsaD-His_6, linking PS I to the surface (Figure 4-3-c).[14] Photocurrents were established, and were enhanced with the addition of V6K and A6K peptides that aided in the stabilization of PS I during the device fabrication.

Ni-NTA was also used to link RCs to gold electrode surfaces. A poly-histidine tag was introduced at the C-terminal end of the M-subunit of RCs that were expressed and isolated from *Rhodobacter sphaeroides* strain SMpHis.[15] These His_7 RCs were then immobilized on Ni-NTA capped gold electrodes (Figure 4-4-a).[15] While a photocurrent was established, the major factors decreasing the efficiency of the electron transfer between the RCs and electrode might be the buried location of the primary donor inside the RC protein complexes. This leads to a rather long electron tunneling distance between the RCs and the electrode, and thus inefficient electron transfer. This problem was addressed in a more recent study that introduced the electron-donating protein, cytochrome c to this His_7 RC system.[16] Horse heart cytochrome c was added to His_7 RCs that were immobilized on Ni-NTA gold electrodes and enhanced photocurrents were

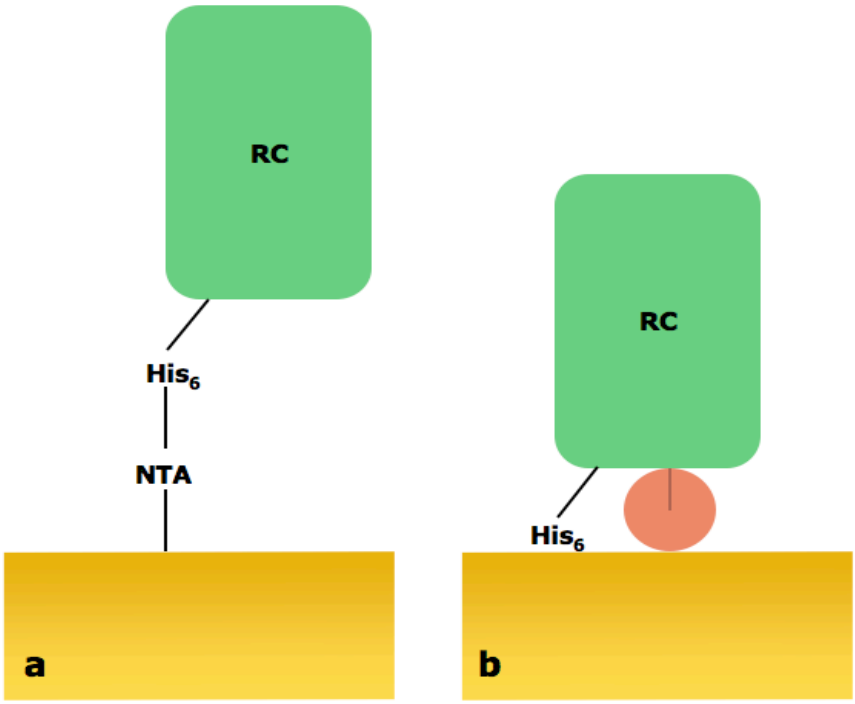

Figure **4-4**: Mutants of bacterial reaction centers from Purple Non-Sulfur bacteria that contained a His_7 tag at the C-terminal of the M subunit were immobilized on gold electrodes by linkage with a Ni-NTA (a). Observed photocurrents were enhanced when horse heart cytochrome c was added. The photocurrent enhancement was attributed to the formation of an electron transfer complex (b).

observed (Figure 4-4-b). This photocurret enhancement can be attributed to either the division of the electron tunneling pathway into two relatively short steps (from SAM to heme and from heme to primary donor) or the possible decrease in the distance of total tunneling by the size of the heme because of electron delocalization within the porphyrin ring.[16] While this study posits that an electron transfer complex is formed between the *R. sphaeroides* RCs and the horse heart cytochrome c that enables the photocurrent enhancement, use of cytochrome c electron transfer proteins that are more closely related to the photosynthetic reaction center proteins may increase

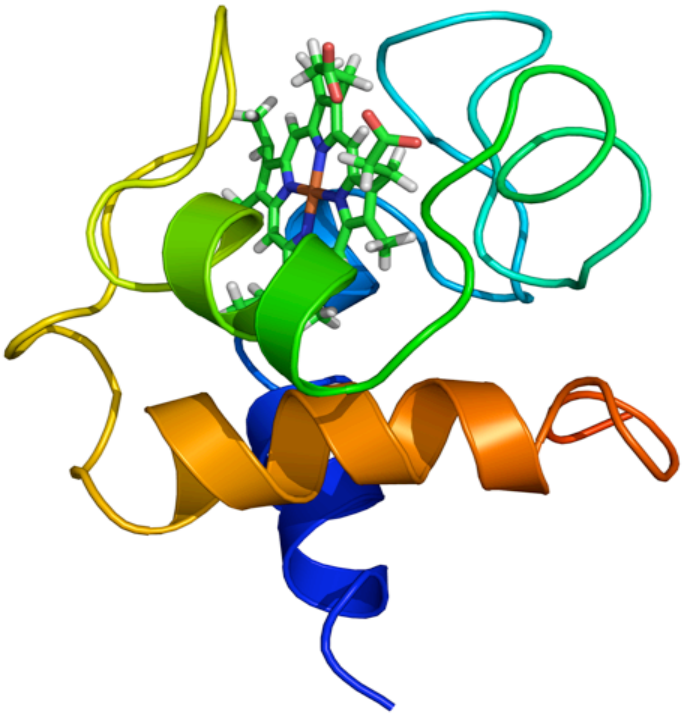

Figure **4-5**: Cytochrome c_6 is a soluble electron transport protein active in the electron transport pathway of Photosystem I in cyanobacteria. This image is an average of 30 NMR lowest energy solution structures of the cytochrome c_6 from *Thermosynechococcus elongatus* (1C6S).

this photoenhancement to an even greater extent as their interfaces have been designed through evolution for specific interactions with one another.

Attachment of Photosystem I Through and Intervening Layer of Cytochrome c_6

Cytochrome c_6 (Figure 4-5), a small (~10 kDa) c-type cytochrome, is a natural electron donor to PS I and is able to transfer electrons to $P700^+$ within 15 μs in solution.[17] This cytochrome is expressed when Cu concentrations are too low to allow for plastocyanin synthesis

```
                ** _****_* *_*** ** * * *_* * ** ***  **  *
Thermo     1 - ADLANGAKVF SGNCAACHMG GGNVVMANKT LKKEALEQFG
Anabaena   1 - ADSVNGAKIF SANCASCHAG GKNLVQAQKT LKKADLEKYG

                *** _*** * *  ******* * ***  ***  *******
Thermo    41 - MYSEDAIIYQ VQHGKNAMPA FAGRLTDEQI QDVAAYVLDQ
Anabaena  41 - MYSAEAIIAQ VTNGKNAMPA FKGRLKPEQI EDVAAYVLGK

                *   *
Thermo    81 - AAKGWAG
Anabaena  81 - ADADWK
```

Figure **4-6**: This amino acid sequence comparison of *Thermosynechococcus elongatus* (*Thermo*) and *Anabaena* sp. PCC 7120 (*Anabaena*) cytochrome c_6 protein shows ~ 66% sequence homology.

in cyanobacteria. Electrostatic interactions and hydrophobic forces between the luminal interface of PS I and the solvent-exposed face of the heme in Cyt c_6 play a role in the proteins coalescing.ref These interactions also play a role in orienting the proteins to bring electron transfer cofactors into proximity to allow for rapid electron transfer. It has also been shown that Cyt c_6 from the cyanobacterium *Synechococcus* sp. PCC 7002 can be chemically cross-linked to the PsaF subunit of PS I using the zero-length cross-linker, 1-Ethyl-3-[3-dimethylaminopropyl]carbodiimide, EDC.

Because of the relatively small size of the protein, and the relatively large heme group that is inserted into a cleft at the surface, when attached to a gold electrode, Cyt c_6 would effectively divide the 30 Å distance from the electrode to $P700^+$ into roughly two equal distances that are 12 to 15 Å. These distances are short enough to allow for sub-millisecond electron transfer from the electrode to $P700^+$ based on the Moser-Dutton ruler.[18] Cross-linking PS I to Cyt c_6 insures rapid and efficient electron transfer from the electrode to $P700^+$ as the electron transfer would not depend on the rates of binding, release, and diffusion from the electrode surface.

The same lysine residues that are located near the heme that play a role in the interactions with PS I are also responsible, traditionally, for orienting the Cyt c_6 on metal surfaces. Because these residues need to be free to interact with PS I, a variant needed to be constructed to allow for the correct orientation on the electrode surface.

Cyt c_6 from *Anabaena* 7120 has a high sequence homology to Cyt c_6 from *Thermosynechococcus elongatus* and therefore is expected to have a similar structure (Figure 4-6). The C-terminal of the protein consists of a highly flexible tail attached to an α-helix that lies at the opposite side of the protein form the heme.

A variant of Cyt c_6 has been constructed that introduces a cysteine residue on C-terminal at position 83 (Ala $\rightarrow$ Cys) and incorporates another following the last amino acid, creating position 87. Insertion of these cys residues will provide for the formation of a covalent bond between the Au electrode surface and the protein via Au-S bonds (Figure 4-7-a). Introduction of two cys residues imparts bidentate ligand properties to the protein. The strength of these covalent bonds is greater than that of the interactions that control Cyt c_6 electrostatic adsorption on Au electrode surfaces, thus making this orientation thermodynamically favorable. The Au-S bond formation results in Cyt c_6 bound the electrode surface in a favorable orientation for interactions with PS I. In this orientation the heme is located ~12 Å from the electrode surface. Additionally, the thiol groups of the introduced cys residues can be selectively bound to an alkanethiol SAM with a maleimide functionality. This maleimide reactive group selectively forms covalent bonds with thiol groups, like those introduced into the C-terminal of the Cyt c_6 protein (Figure 4-7-b).

This study takes the initial steps toward forming a functional device by investigating the attachment of PS I on gold electrodes by means of a variety of strategies including physisorption onto alkanethiol SAMs and lays the ground work for the covalent attachment of PS I via EDC cross-linking to ammine-terminated SAMs or mediated through both native and variant cytochrome c_6.

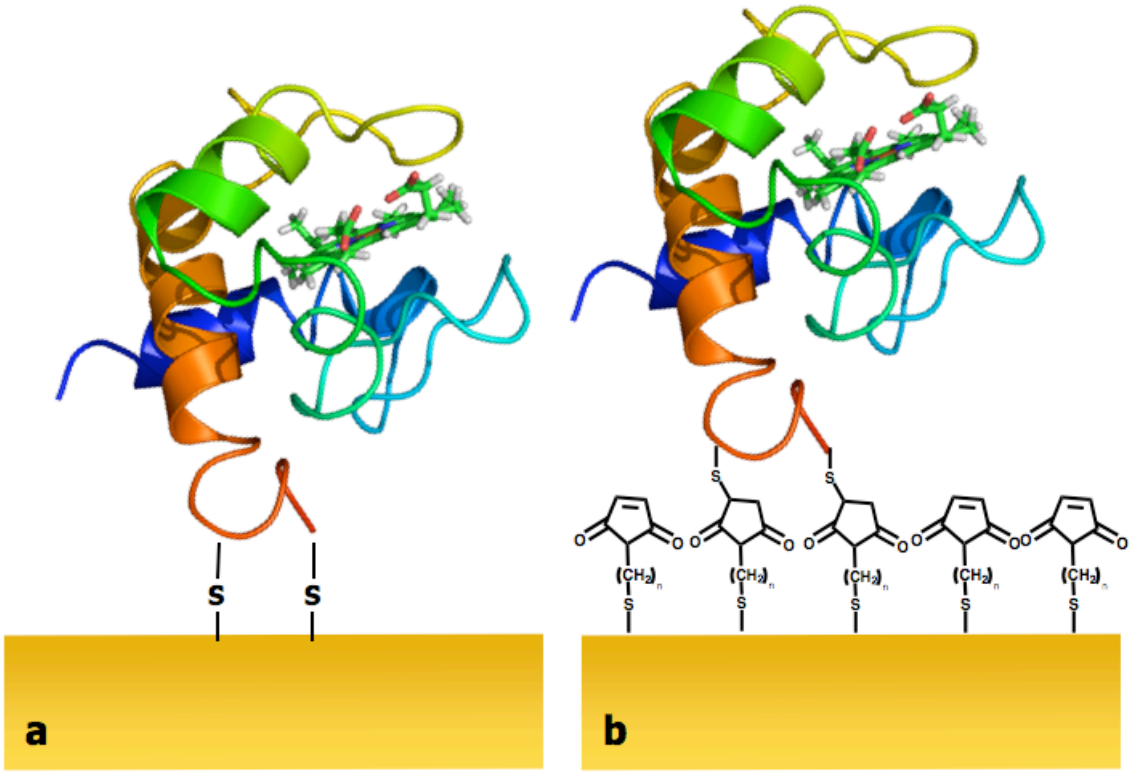

Figure **4-7**: Cytochrome c_6 variants may be attached directly to the gold electrode by Au-S bonds with the introduced cysteine residues (a) or selectively bound to maleimide terminated SAM (b).

Materials and Methods

Materials

All chemicals were used as purchased, without further modification. All solutions were prepared with 18.1 MΩ doubly distilled water or reagent grade organic solvents. ITO coated glass slides (1 x 3 inch) were purchased from Sigma Aldrich. DNA primers for construction of the cytochrome c_6 variants were obtained from Integrated DNA Technologies. Following purification, proteins were stored at -80 °C.

Substrate Preparation

ITO coated glass slides were cleaned first cleaned to prepare for gold deposition. Gold deposition on ITO coated glass slides was achieved by first evaporating a 50 Å layer of chromium to aid in adhesion, followed by a 1000 Å layer of gold at a base pressure of 3×10^{-6} Torr using a Semicore electron beam metal evaporator deposition chamber. The gold-coated slides were then cut into 1cm x 2.5 cm strips.

Site-directed Mutagenesis of Cytochrome c_6 from *Anabaena* sp. PCC 7120

The DNA fragment containing the *Anabaena* sp. PCC 7120 *petJ* gene, which encodes cytochrome c_6, was amplified through standard polymerase chain reaction (PCR) techniques from *Anabaena* 7120 chromosomal DNA. The *petJ* gene was cloned into the pET42b expression vector to enable overproduction of cytochrome c_6 in *E. coli* cells and the sequence of the vector was verified by DNA sequencing.

The mutant *petJ* gene was constructed by PCR using primers of 34 or 31 bases, 15 ng DNA template, and 15 minute extension time. The forward primer, 5' – GCA CAT TGG AAG TGT TAA ATT CCA CTT CAA GAG C – 3' and reverse primer 5' – GCT CTT GAA GTG GAA TTT AAC ACT TCC AAT CTG C – 3' were designed from the DNA sequence to introduce the TGT codon to insert a cysteine amino acid residue at the end of the cytochrome c_6 protein when expressed. The forward primer, 5' – GCC GAT TGT GAT TGG AAG TGT TAA ATT CCA C – 3' and the reverse primer, 5' – GTG CAA TTT AAC ACT TCC AAT CAC AAAT CGG C – 3' were designed from the DNA sequence to introduce a TGT cysteine codon at position 83 in the cytochrome c_6 amino acid sequence. DNA sequencing and DNA agarose gel electrophoresis verified the mutant petJ gene with the TGT codon at position 83 and the newly

introduced position 87 in the pET42b expression vector. The Penn State Nucleic Acids Facility carried out all nucleotide sequencing.

Purification of Photosystem I Complexes from *Synechcoccus* sp. PCC 7002

PS I complexes were purified from *Synechococcus* sp. PCC 7002 thylakoids using established methods.[19] PS I complexes were isolated by detergent treatment of fragmented thylakoid membranes using 1% Triton X-100 and purified by sucrose density ultracentrifugation. The PS I complexes were resuspended in buffer containing 0.1% Triton X-100 and 15% glycerol in 50 mM Tris buffer, pH 8.3.

Surface Functionalization

The gold-coated strips of ITO coated glass slides were thoroughly rinsed with ethanol and dried in a stream of N_2. The substrate was then immersed in a 1 mM solution of alkanethiol in ethanol for 6 hours at room temperature. After removal from the solution, the sample was rinsed with ethanol and dried in a stream of N_2. PS I solutions (10 μg Chl mL^{-1} final concenration) were prepared in 50 mM Tris (pH 8.3), 20 mM NaCl, and 0.1% Triton X-100. SAM-coated gold substrates were immersed in the dilute PS I solution at 4 °C for 24 hours. After adsorption, the samples were thoroughly rinsed with the buffer solution (50 mM Tris (pH 8.3), 20 mM NaCl, 0.1% Triton X-100), and either dried in a stream of N_2 for ellipsometric or AFM characterization or analyzed immediately for photocurrent measurements.

Ellipsometric Measurements

Ellipsometric analysis of SAM and PS I layers was obtained using a Gaertner L116 Variable Angle Ellipsometer. Measurements were made with a beam angle of 70° using a Helium-Neon laser with λ_{max} of 632.8 nm. The relative refractive index of the gold substrate (N_S) was determined to be 0.091 and the extinction value refractive index of the substrate (K_S) was determined to be -3.426 and these values were used for determining layer thicknesses.

AFM Imaging

AFM images were obtained using a Digital Instruments Dimension 3100 Atomic Force Microscope operated in tapping mode. Silicon probes were chosen with a tip radius <10 nm mounted on a single beam cantilever. A 1.0 μm x 1.0 μm area of the gold surface was imaged in air at room temperature with a horizontal scan rate of 1.2 Hz and 256 samples per line.

Data analysis was performed using WSXM 4.0 software for providing height patterns and cross-section profiles. Images were obtained from random spot surface sampling. All images were reproducible.

Results and Discussion

***Anabaena* sp. PCC 7120 *petJ* Gene Mutagenesis Verification**

DNA nucleotide sequencing revealed the presence of the inserted TGT codons corresponding to positions 83 and 87 in the amino acid sequence of cytochrome c_6 (Figure 4-8-a). DNA agarose gel electrophresis confirmed the expression vector PCR products (Figure 4-8-b).

Overproduction in *E. coli* (BL21 DE3) cells by coexpression with the pEC 86 (ccm gene) expression vector has yet to be confirmed.

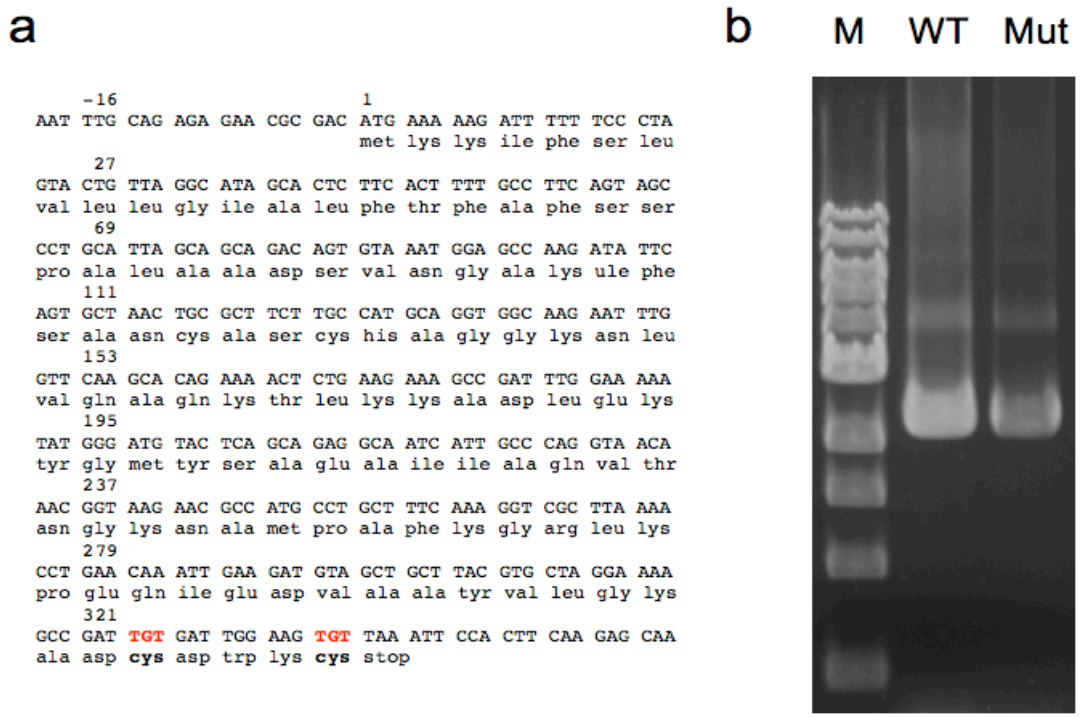

Figure **4-8**: Nucleotide sequence (coding strand) and deduced amino acid sequence of cytochrome c_6 (a) obtained from sequencing results. Agarose gel electrophoresis of the *petJ* gene in the pET42b vector (b). Lane M corresponds to the DNA molecular weight marker, lane WT to the wild type *petJ* in the vector, and lane Mut to A83C/87C mutant *petJ* in the vector.

Ellipsometric Measurements

Ellipsometric measurements were obtained for PS I that had been adsorbed on a variety of alkanethiol SAMs with various ω-functionalities (Table 4-1). These end groups control the adsorption of PS I on the gold surface. A PS I layer thickness of 0.44 Å was observed for the methyl terminated SAM. This indicates that little or no PS I was able to adsorb onto this SAM.

This is most likely due to the highly hydrophobic surface of the methyl terminated SAM. PS I is surrounded by a surfactant layer (Triton X-100) which has highly hydrophilic head groups and the stromal and lumenal interfaces of PS I also display hydrophilic characteristics. Adsorption is hindered by the incompatibility of these hydrophilic surfaces and the hydrophobic methyl-terminated SAM.

PS I adsorption was observed for all of the other SAMs as their ω-functionalities are hydrophilic. The thickest layer of PS I was observed on the amine-terminated monolayer, with a layer thickness of 56.07 Å. This thickness may indicate full monolayer coverage, given that the thickness of PS I through the membrane is ~ 50 Å by crystallographic analysis.[20] PS I layer thicknesses of 26.64 and 36.64 Å were observed for the hydroxyl and carboxyl terminated SAMs, respectively. This layer thickness could indicate protein denaturation as the thickness is less than 50 Å, or it could indicate incomplete PS I monolayer formation as ellipsometry is a technique that looks at the average thickness of layers over a given surface area. Atomic Force Microscope analysis can determine whether protein denaturation or incomplete monolayer formation is the cause of the lower measured layer thicknesses.

Table **4-1**: Alkanethiol SAM and Photosystem I layer thicknesses measured on a 1000 Å gold layer as determined by Ellipsometric analysis.

	SAM Thickness	SAM and PS I Thickness	PS I Layer Thickness
6-mercapto-1-hexanol	7.14	33.78	26.64
Mercaptohexanoic acid	8.28	44.92	36.64
11-amine-undecanethiol	14.21	70.28	56.07
Hexanethiol	7.77	8.21	0.44

Atomic Force Microscope Imaging

Atomic Force Microscope images of bare gold, SAMs composed of 6-mercapto-1-hexanol, mercaptohexanoic acid, and 11-amine-undecanethiol, and PS I adsorbed on these SAMs were obtained (Figure 4-9). The bare gold surface was found to be relatively flat (Figure 4-9-a). Images of the SAMs (Figure 4-9-b,d,f) show similar surface characteristics to the bare gold, while the samples in which PS I had been introduced (Figure 4-9-c,e,g) show an increase in surface roughness, which indicates protein adsorption. Cross-section profiles of these images follow the trace of the blue line in the corresponding image and indicate average PS I protein layer thicknesses of ~6 nm which indicates that the PS I has not denatured on the surface. The AFM profiles indicate that instead of PS I denaturing on theses surfaces, incomplete monolayers of PS I result in the < 5 nm layer thicknesses measured by ellipsometry.

Conclusions

Steps have been made toward the construction of a functional device by the adsorption of PS I on gold electrode surfaces. The Ellipsometric and AFM data qualitatively show that cyanobacterial PS I is able to functionalize alkanethiol SAMs with hydroxyl, carboxyl, and amine ω-functionalities, but is unable to functionalize a SAM with a hydrophobic methyl ω-functionality. The hydrophilic characteristics of the solubolized protein complexes are the largest contributing factors for their ability for functionalize these surfaces.

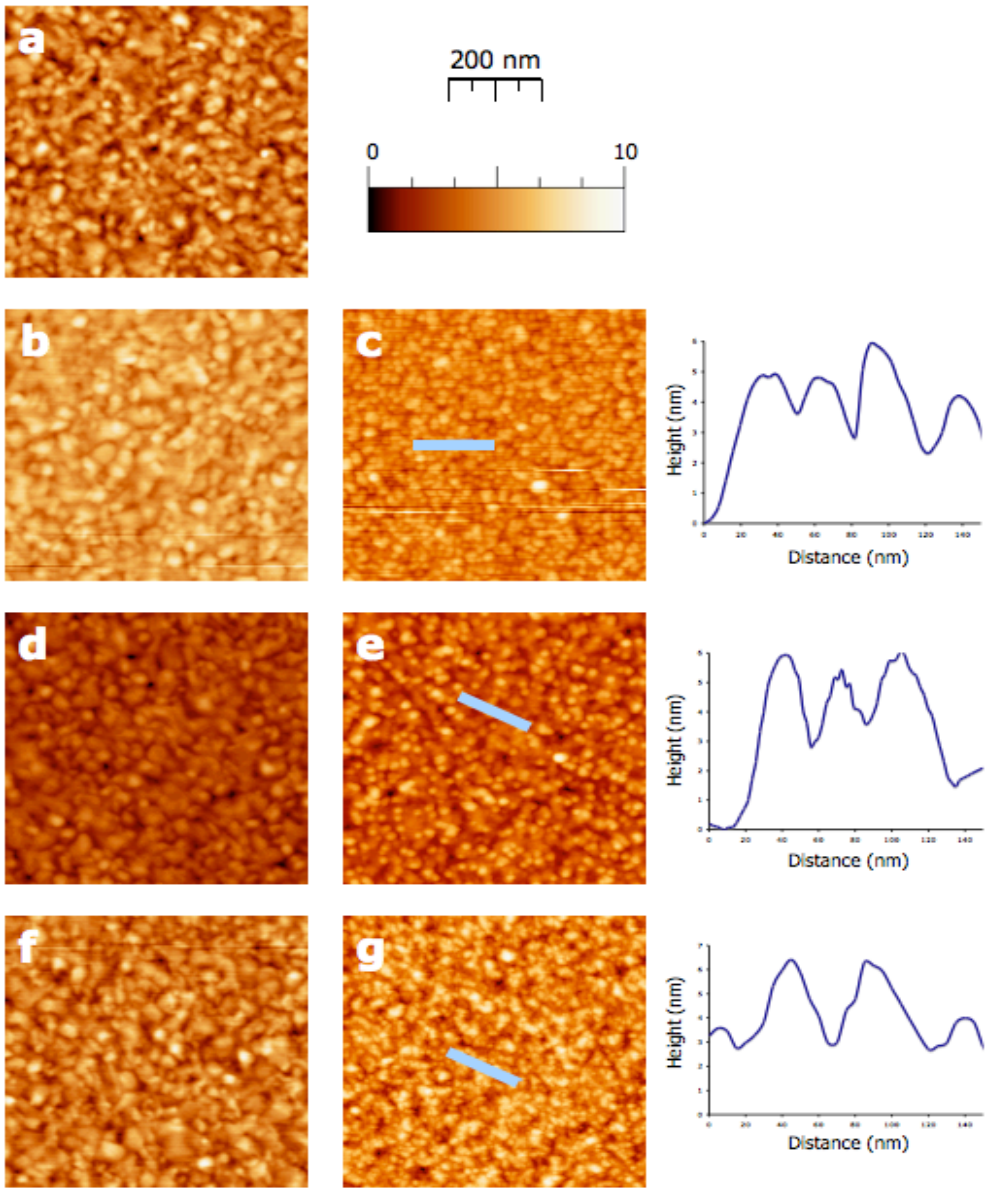

Figure **4-9**: Tapping mode AFM images of gold coated ITO glass slides were obtained for bare gold (a), mercaptohexanoic acid (b), mercaptohexanol (d), and 11-amino-undecanethiol (f) functionalized gold surfaces. PS I adsorbed on mercaptohexanoic acid (c), mercaptohexanol (e), and 11-amino-undecanethiol (f) was also imaged. Profile plots (right) follow the blue line in (c), (e), and (g), respectively. All images are 1.0 μm x 1.0 μm, and the scale bar is 200 nm.

Future Directions

While the adsorption of PS I on alkanethiol-capped gold surfaces has been addressed qualitatively, quantitative measurements will be made via Quartz Crystal Microbalace (QCM) gravitmetric analysis to elucidate the surface coverage of PS I on the 6-mercapto-1-hexanol, mercaptohexanoic acid, and 11-amine-undecanethiol SAMs. Additionally, PS I adsorption and EDC cross-linking to mixed monolayers composed of 6-mercapto-1-hexanol or mercaptohexanoic acid with 11-amine-undecanethiol will be evaluated via Ellipsometry, AFM, and QCM measurements.

Photocurrent measurements of PS I on all of these SAMs will be completed by evaluating the current generated when white light is allowed to illuminate the PS I/electrode assemblies. These measurements may be made by immersing the PS I electrode assemblies in a solution containing 100 mM methyl viologen as an electron accepting species and illuminating the electrode assemblies with actinic white light. When illuminated, PS I will promote electrons, donate these electrons to the methyl viologen in solution, and take electrons from the electrode to establish the photocurrent. Additionally, both the variant and wild type cytochrome c_6 may be introduced to these PS I/electrode assemblies to evaluate any possible increases in photocurrent performance that may be gained.

Spinach PS I was shown to increase the overall efficiency of the PS I/molecular wire/Pt nanoparticle bioconjugates. It may also be possible to increase the efficiency of this device with the use of Spinach PS I. Due to the smaller size of the PS I reaction centers from spinach, a higher surface coverage may be achieved, leading to a possible increase in measured photocurrents and therefore a possible increase in the H_2 production in the assembled device.

References

1. Grimme, R.A., Lubner, C.E., Bryant, D.A., Golbeck, J.H., *J. Am. Chem. Soc.*, **2008**, 130, 6308-6309.
2. Grimme, R.A., Lubner, C.E., Golbeck, J.H., *Dalton Trans.,* **2009** (submitted).
3. A Ko, B.S., Babcock, B., Jennings, G.K., Tilden, S.G., Peterson, R.R., Cliffel, D., Greenbaum, E., *Langmuir*, **2004**, 20, 4033-4038.
4. B Lee, I., Lee, J.W., Greenbaum, E., *Phys. Rev. Lett.*, **1997**, 79, 3294-3297.
5. C Ciobanu, M., Kincaid, H.A., Lo, V., Dukes, A.D., Jennings, G.K., Cliffel, D.E., *J. Electroanal. Chem.*, **2007**, 599, 72-78.
6. D Lee, I., Lee, J.W., Stubna, A., Greenbaum, E., *J. Phys. Chem.*, **2000**, 104, 2439-2443.
7. E Kincaid, H.A., Neidringhaus, T., Coubanu, M., Cliffel, D.E., Jennings, G.K., *Langmuir*, **2006**, 22, 8114-8120.
8. F Faulkner, C.J., Lees, S., Ciesielski, P.N., Cliffel, D.E., Jennings, G.K., *Langmuir*, **2008**, 24, 8409-8412.
9. G Ciesielski, P.N., Scott, A.M., Faulkner, C.J., Berron, B.J., Cliffel, D.E., Jennings, G.K., *Nano*, **2008**, 2, 2465-2472.
10. H Terasaki, N., Yamamoto, N., Higara, T., Sato, I., Inoue, Y., Yamada, S., *Thin Solid Films*, **2006**, 499, 153-156.
11. I Terasaki, N., Yamamoto, N., Tamada, K., Hattori, M., Hiraga, T., Tohri, A., Sato, I., Iwai, M., Iwai, M., Taguchi, S., Enami, I., Inoue, Y., Yamanoi, Y., Yonezawa, S., Minakata, M., Ohmori, T., Saki, M., Fujii, M., *Biochim. Biophys. Acta*, **2007**, 1767, 653-659.
12. J Frolov, L., Rosenwaks, Y., Carmeli, C., Carmeli, I., *Adv. Mater.*, **2005**, 17, 2434-2437.

13. K Carmeli, I., Frolov, L., Carmeli, C., Richter, S., *J. Am. Chem. Soc.*, **2007**, 129, 12352-12353.

14. Das, R., Kiley, P.J., Segal, M., Norville, J., Yu, A.A., Wang, L., Trammell, S.A., Reddick, L.E., Kumar, R., Stellacci, F., Lebedev, N., Schnur, J., Bruce, B.D., Zhang, S., Baldo, M., *Nano Lett.*, **2004**, 4, 2345-2349.

15. Trammell, S.A., Wang, L., Zullo, J.M., Shashidar, R., Lebedev, N., *Biosens. Bioelectron.*, **2004**, 19, 1649-1655.

16. Lebedev, N., Trammell, S.A., Spano, A., Lukashev, E., Griva, I. Schnur, J., *J. Am. Chem. Soc.*, **2006**, 128, 12044-12045.

17. Diaz, A., Navarro, F., Herds, M., Navarro, J.A., Chavez, S., Florencio, F.J., De la Rosa, M.A., *FEBS Lett.*, **1994**, 347, 173-177.

18. Moser, C.C., Dutton, P.L., *Biochim. Biophys. Acta*, **1992**, 1101, 171-176.

19. G. Z. Shen, J. D. Zhao, S. K. Reimer, M. L. Antonkine, Q. Cai, S. M. Weiland, J. H. Golbeck and D. A. Bryant, *J. Biol. Chem.*, 2002, **277**, 20343-20354.

20. Jordan, P., Fromme, P., Witt. H.T., Klukas, O., Saenger, W., Krauss, N., *Nature*, **2001**, 6840, 909-917.